AD-A224 273

DTIC FILE COPY

NWC TP 7074

A Planar Rocket Motor Model for Visualization of Violent Reaction Due to Fragment Impact

by
S. A. Finzegan
J. K. Pringle
J. C. Schulz
and
M. D. Alexander
Research Department

MAY 1990

NAVAL WEAPONS CENTER
CHINA LAKE, CA 93555-6001

DTIC
ELECTE
JUL 2 0 1990
S

Naval Weapons Center

FOREWORD

The research described in this report was performed at the Naval Weapons Center during fiscal years 1989 and 1990 as part of an effort to understand the propellant reactions occurring at the inner bore of a rocket motor. The results also serve to demonstrate the utility of the planar rocket motor model as a research tool. This effort was supported with funds from the Insensitive Munitions Advanced Development Program, Program Element 63609-N-Subproject S0363 and also from Independent Research funds. Advanced development support of theoretical, experimental, and analytical work related to reactive behavior of explosives and propellants is essential to development of a utile technology base for the design of insensitive munitions.

Approved by
R. L. DERR, *Head*
Research Department
26 March 1990

Under authority of
D. W. COOK
Capt., U.S. Nav
Commander

Released for publication by
W. R. PORTER
Technical Director

NWC Technical Publication 707[illegible]

Published by.....Technical Information Department
Collation.....Cover, 27 leaves
First printing.....[illegible]

REPORT DOCUMENTATION PAGE

Form Approved
OMB No. 0704-0188

Public reporting burden for this collection of information is estimated to average 1 hour per response, including the time for reviewing instructions, searching existing data sources, gathering and maintaining the data needed, and completing and reviewing the collection of information. Send comments regarding this burden estimate or any other aspect of this collection of information, including suggestions for reducing this burden, to Washington Headquarters Services, Directorate for Information Operations and Reports, 1215 Jefferson Davis Highway, Suite 1204, Arlington, VA 22202-4302, and to the Office of Management and Budget, Paperwork Reduction Project (0704-0188), Washington, DC 20503.

1. AGENCY USE ONLY *(Leave blank)*	2. REPORT DATE MAY 1990	3. REPORT TYPE AND DATES COVERED Research; September 1989 - January 1990

4. TITLE AND SUBTITLE
A Planar Rocket Motor Model for Visualization of Violent Reaction Due to Fragment Impact

5. FUNDING NUMBERS

6. AUTHOR(S)
S. A. Finnegan, J. K. Pringle, J. C. Schulz, M. D. Alexander

7. PERFORMING ORGANIZATION NAME(S) AND ADDRESS(ES)
Naval Weapons Center
China Lake, California 93555-6001

8. PERFORMING ORGANIZATION REPORT NUMBER
NWC TP 7074

9. SPONSORING/MONITORING AGENCY NAME(S) AND ADDRESS(ES)

10. SPONSORING/MONITORING AGENCY REPORT NUMBER

11. SUPPLEMENTARY NOTES

12a. DISTRIBUTION/AVAILABILITY STATEMENT
Approved for public release; distribution is unlimited.

12b. DISTRIBUTION CODE

13. ABSTRACT *(Maximum 200 words)*

A planar model of a rocket motor with an inner bore has been developed to study reaction mechanisms associated with fragment impact. The open architecture of the model allows impact reaction events in the bore region to be recorded photographically. Results from gun firings of steel spheres against planar rocket motor models are presented that demonstrate the utility of the planar model as a research tool. Possible use of the model as a propellant screening test is also discussed.

14. SUBJECT TERMS
Ballistic impact, Propellant reaction, XDT, BVR, Rocket motor, Planar model, Violent reaction

15. NUMBER OF PAGES
52

16. PRICE CODE

17. SECURITY CLASSIFICATION OF REPORT	18. SECURITY CLASSIFICATION OF THIS PAGE	19. SECURITY CLASSIFICATION OF ABSTRACT	20. LIMITATION OF ABSTRACT
UNCLASSIFIED	UNCLASSIFIED	UNCLASSIFIED	SAR

NSN 7540-01-280-5500

Standard Form 298 (Rev. 2-89)
Prescribed by ANSI Std. 239-18
298-102

CONTENTS

Abstract 3

Introduction 3

Experimental Setup 5

Firing Matrix 7

Photographic Results 8
- HTPB/AP Propellant 9
- HEP-1 Propellant 15
- HEP-2 Propellant 16

Conclusions 19

Recommendations 19

References 21

Appendixes:
- A. Detailed Table of Test Configurations and Results 23
- B. Photographic Sequences for all Tests 27

Figures:
1. Planar Rocket Motor Model 4
2. Photograph of Test Setup 5
3. Close-up of Target Area 6
4. Numbering Order for High-Speed Photographs 8
5. Sketch of Debris Bubble Ignition Process 10
6. Sketch of Propellant Debris Flow/Reaction Patterns 11
7. Sketch of Crater Ejecta Reaction Pattern 13

DTIC COPY INSPECTED 5

sion For
GRA&I ☑
TAB ☐
unced ☐
ication
bution/
lability Codes
Dist | Avail and/or Special
A-1

8. Detonation Delay Times for HEP-2 Propellant (Tests 16 Through 22) 17
9. Sketch of XDT Reaction Process 18
B-1. Photographic Sequence for Test 1 28
B-2. Photographic Sequence for Test 2 29
B-3. Photographic Sequence for Test 3 30
B-4. Photographic Sequence for Test 4 31
B-5. Photographic Sequence for Test 5 32
B-6. Photographic Sequence for Test 6 33
B-7. Photographic Sequence for Test 7 34
B-8. Photographic Sequence for Test 8 35
B-9. Photographic Sequence for Test 9 36
B-10. Photographic Sequence for Test 10 37
B-11. Photographic Sequence for Test 11 38
B-12. Photographic Sequence for Test 12 39
B-13. Photographic Sequence for Test 13 40
B-14. Photographic Sequence for Test 14 41
B-15. Photographic Sequence for Test 15 42
B-16. Photographic Sequence for Test 16 43
B-17. Photographic Sequence for Test 17 44
B-18. Photographic Sequence for Test 18 45
B-19. Photographic Sequence for Test 19 46
B-20. Photographic Sequence for Test 20 47
B-21. Photographic Sequence for Test 21 48
B-22. Photographic Sequence for Test 22 49
B-23. Photographic Sequence for Test 23 50

Table:

A-1. Detailed Results for Planar Rocket Motor Model Test Firings 24

ABSTRACT

A planar model of a rocket motor with an inner bore has been developed to study reaction mechanisms associated with fragment impact. The open architecture of the model allows impact and reaction events in the bore region to be recorded photographically. Results from gun firings of steel spheres against planar rocket motor models are presented that demonstrate the utility of the planar model as a research tool. Possible use of the model as a propellant screening test is also discussed.

INTRODUCTION

Bullet or fragment impact against cased propellant can cause an explosive reaction through a number of mechanisms. The initial pressure transient may produce immediate reaction through shock-to-detonation transition (SDT). Gross deformation and damage to the energetic material by a perforating fragment may lead to reaction at a somewhat later time. Delayed mechanisms as a whole can be lumped under the heading, burn-to-violent reaction (BVR) (Reference 1). Delayed, impact-induced mechanisms that lead to detonation are usually described as X (unknown mechanism)-to-detonation transition (XDT) reactions (Reference 2).

Study of delayed reaction phenomena is complicated by the fact that these processes occur within the motor case and therefore are not visible from outside. A previous report describes an inert, planar rocket motor model that was used to study debris cloud formation at an inner bore resulting from fragment impact (Reference 3). The model consists of a steel plate, a propellant simulant layer, an air gap, a second propellant simulant layer, and a second steel plate, as shown in Figure 1. If the simulant is replaced with live propellant, this planar rocket motor model can be used to study reaction phenomena associated with fragment impact.

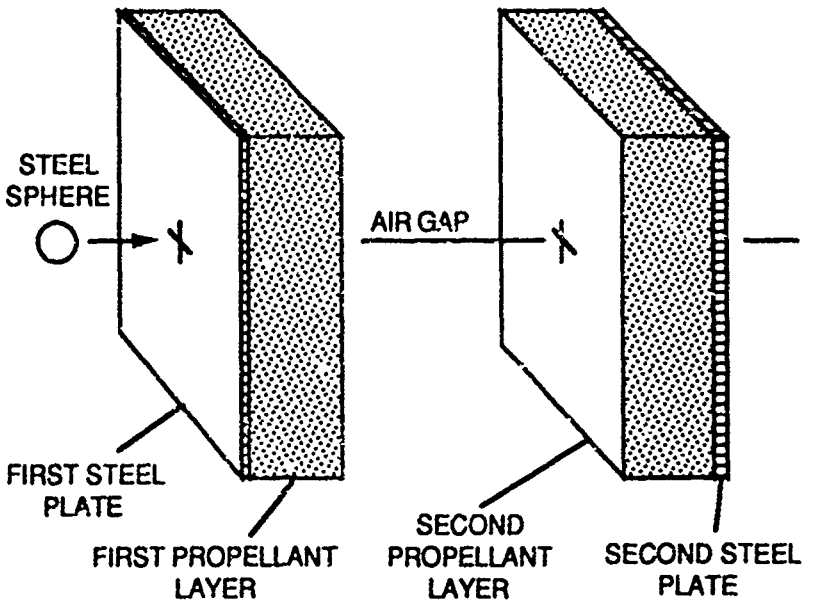

FIGURE 1. Planar Rocket Motor Model.

Because the bore (air gap) in the model is open rather than enclosed by a cylindrical case, this region can be viewed and photographed with a high speed camera during an impact test. Thus, the burning and violent reaction processes (including ignition sites, reaction velocities, etc.) can be observed in the film records after the test and can be characterized in detail. Similar information could, at best, only be inferred from indirect measurements (e.g., pressure, temperature, light, motion, debris sizes, and debris throw distances).

The planar model is, of course, only an approximate representation of an actual rocket motor. Curvature and confinement effects due to the cylindrical geometry of an actual motor have been eliminated. Therefore the results from planar model tests must be regarded as largely qualitative; nevertheless, they provide reaction region data that cannot be obtained any other way.

This report describes a set of experiments involving gun firings of steel spheres against planar rocket motor model targets. Three different propellants (and also a simulant material) were used. Tests were conducted over a wide range of motor bore sizes. In addition to providing information as to the types of inner bore reactions likely in these propellants, the results serve, more generally, to demonstrate the utility of the planar rocket motor model as a research tool.

The tests documented in this report can be viewed as a continuation of the inert simulant, ballistic tests of Reference 3. These previous tests showed that projectiles

exiting the rear surface of a propellant layer (inner bore) may produce a large cloud of ejected propellant debris (debris bubble) and that ejection and breakup of propellant material may be inhibited by the presence of a second propellant layer spaced a short distance away (far side of bore). It was suggested in Reference 3 that the additional burn surface associated with the ejected material plays an important role in subsequent BVR mechanisms. The purpose of the present tests was to examine this role using the planar rocket motor model.

EXPERIMENTAL SETUP

The experimental setup has been used in projectile firings over the past several years. A smooth-bore 20mm Mann barrel is attached to a Navy gun mount with a large base and a heavy mass. The mass reduces the recoil and stabilizes the gun for the critical aiming needed in these tests. The position of the gun, along with all of the other components of the test setup, is shown in Figure 2.

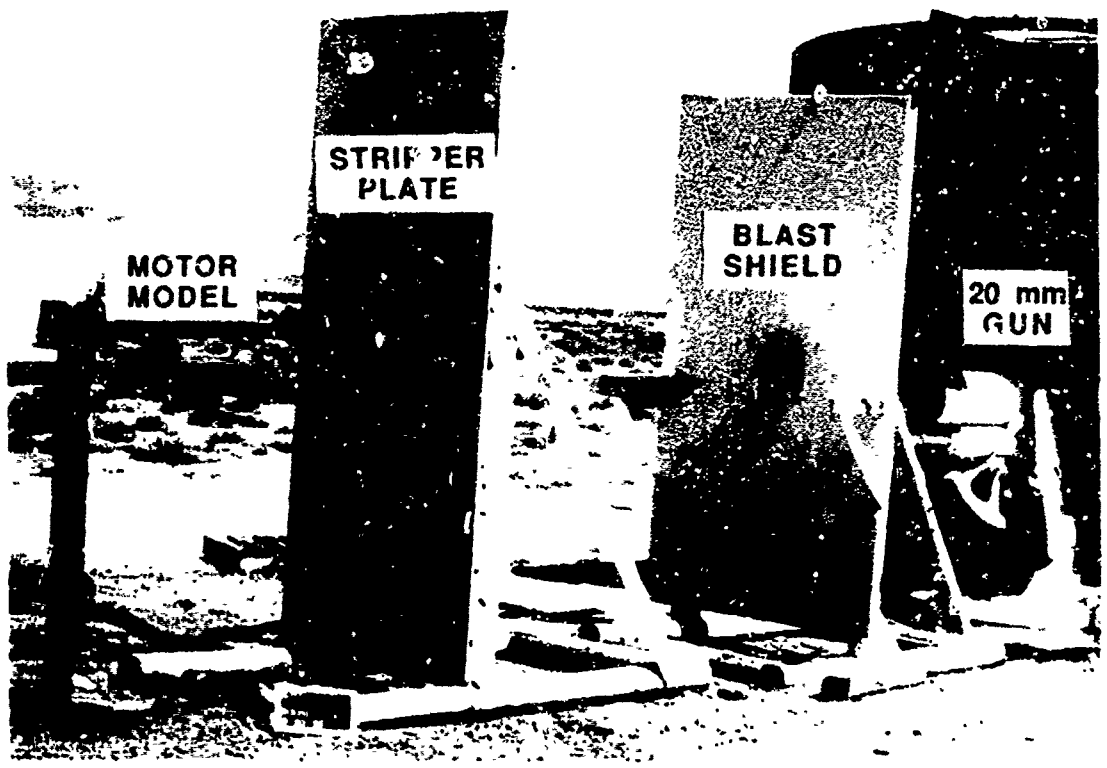

FIGURE 2. Photograph of Test Setup.

Downrange from the gun, two blast shields 6 to 8 feet apart protected the gun from violent reaction in the test item (blast and fragments from a pressure buildup or delayed detonation). These shields were also used as stripper plates to stop the sabots. All projectiles were 3/4-inch-diameter mild steel spheres, saboted so they could be fired in a 20mm gun. For these tests, all of the rounds were loaded with 19 grams of DuPont IMR 4198 powder. This powder load gave consistent velocities of approximately 3800 to 3900 ft/s.

A diffusing screen with reference lines on it was placed between the two blast shields. This screen was used in conjunction with a Photec high-speed camera running at 16,000 frames per second to determine projectile velocities.

The planar rocket motor model target was placed approximately one foot beyond the second blast shield and directly in front of a second diffusing screen. This screen along with a Fastax high-speed camera running at 32,000 frames per second was used to record the projectile impact on the front surface of the target and the subsequent reactions within. Figure 3 shows a target in place on a wooden stand with a diffusing screen behind it.

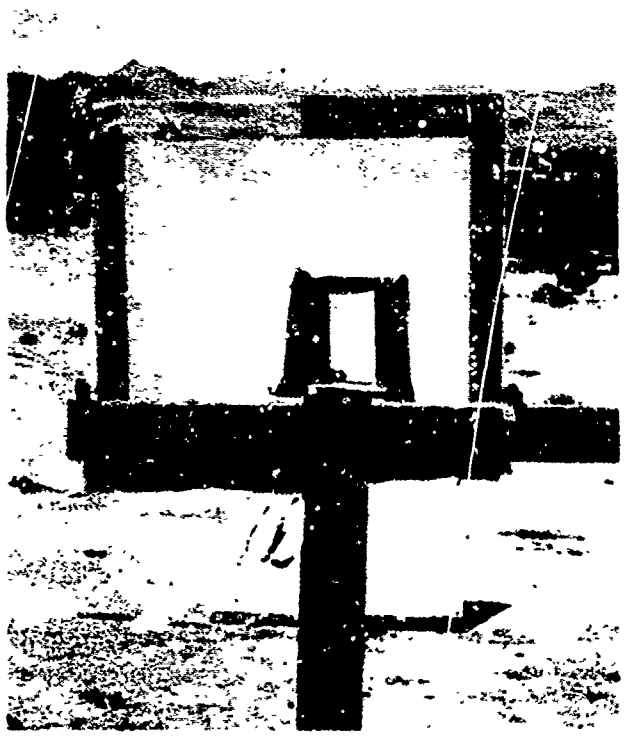

FIGURE 3. Close-up of Target Area.

Projectiles were captured in a bundle of Celotex placed approximately 20 feet downrange from the target. A 1-inch steel plate, located further downrange, served as an additional projectile barrier. After the entire test series was completed, the Celotex bundle was dismantled and most of the projectiles were recovered for examination.

Two large flat mirrors, located some distance behind the experimental setup, were oriented to reflect sunlight onto the two diffusing screens. Because of the continually-changing position of the sun, final adjustments were made just prior to each test. Even with this procedure, illumination was nearly lost for a few of the tests

FIRING MATRIX

The thickness of the propellant layers in the planar model was 1.5 inches for most of the tests (see Figure 1). The lateral dimensions varied from approximately 3 to 7 inches because scrap material was used for many of the tests. It is felt that this variability did not have a significant effect on the test results. The end plates were mostly 1/16-inch, 4130 steel hardened to 370 BHN (Brinell hardness number), although 1/16-inch mild steel was used in a few targets. The air gap between the two propellant layers varied from between 0.25 to 7 inches.

A degree of lateral confinement was provided to the targets by the addition of Plexiglas side walls. The use of Plexiglas allowed unobstructed viewing of propellant reactions within the air gap. Only three tests were conducted without this confinement: one to determine the influence of confinement and the other two to study debris bubble expansion and breakup processes over larger distances (i.e., without the second half of the target).

Three different propellants were tested, HTPB/AP (Class 1.3) and two high energy propellants (Class 1.1). These latter propellants were designated HEP-1 and HEP-2 in this report to avoid potential classification problems. In addition, the HTPB/AP simulant used in Reference 3 was also tested.

HTPB/AP was selected as a baseline propellant because of its wide usage, ready availability, safety (nondetonable under normal impact conditions), ease of ignition, and because it has been extensively studied under dynamic loading conditions (Reference 4). HEP-1 was an EMCDB propellant; only two tests were conducted with this material. HEP-2 contained RDX, HMX, and high energy

plasticizers. A delayed detonation process (XDT) was observed in some tests of this material.

Twenty-three firings were conducted. The target configuration for each test is given in Table A-1. The tests are not listed in chronological order, but are grouped by propellant and for ease of discussion.

PHOTOGRAPHIC RESULTS

A detailed tabulation of high-speed camera results is contained in Table A-1. Sequences of 12 high-speed frames from each test, showing the various impact and reaction events, are contained in Figures B-1 through B-23. References to frame numbers in the text are keyed to Figure 4. Time between successive frames ranged from 27 to 29 microseconds.

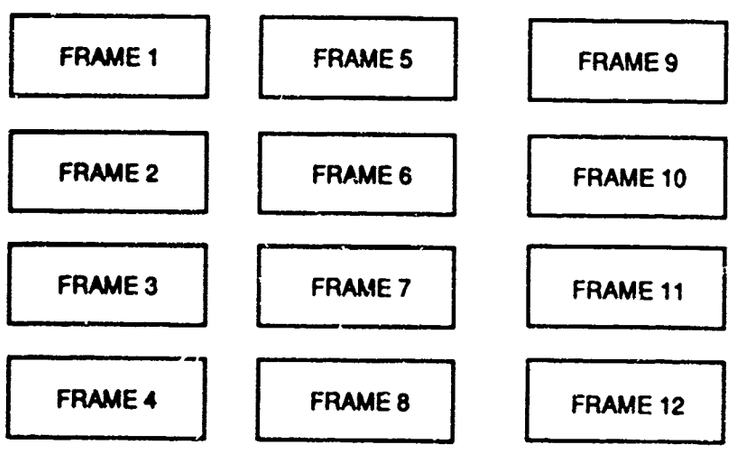

FIGURE 4. Numbering Order for High-Speed Photographs.

Film quality varied considerably from test to test. Incorrect mirror positioning in some tests caused loss of illumination or allowed sunlight to reflect into the camera lens. Occasional camera misalignment makes it appear as though the target was not aligned properly with respect to the gun.

It should be emphasized that the events described in this report are short-lived (a millisecond or less). They represent BVR phenomena caused by fragment or

bullet impact through the center bore of a rocket motor. The words that are used to describe reactions (e.g., "combustion" or "burning") refer almost entirely to events associated with BVR and not to the much longer-lived, steady-state burning process that often follows.

HTPB/AP PROPELLANT

Debris Bubble Expansion Process. The appearance of the debris bubble as it expands outward from the rear of the first propellant layer is shown in a series of high-speed photographs of Test 1 in Figure B-1. For this test, the second propellant layer and second steel plate were not used, allowing unlimited expansion of the bubble. The maximum velocity of the propellant debris at the front of the bubble was 2473 ft/s, while the velocity of the projectile was 2611 ft/s.

Initial contact between the projectile and the first steel plate (Frame 2) resulted in an intense, localized flash of light caused by combustion of metal (impact jetting) and ionization of air. These transient phenomena, lasting between 30 and 60 microseconds, commonly occur during impact and are not to be confused with propellant reaction. Some localized, short-lived propellant burning may also have occurred at this time.

Approximately 30 to 60 microseconds after impact (Frame 3), the rear surface of the propellant layer began to expand outward, beginning at the projectile exit point. Initially, the deformed surface (debris bubble) took on a bell-like shape, but with continued expansion it became more tear-shaped (Frames 10 through 12).

At expansion distances less than approximately five inches (starting from the rear surface of the propellant layer), the bubble was opaque; at a distance of approximately six inches (Frame 9), the bubble began to break up along the front edge; and at a distance of approximately eight inches (Frame 11), breakup was substantially complete. Also, at a distance of approximately six inches, the projectile emerged as a distinct object near the front of the bubble and at greater distances (Frames 10 through 12), began to outdistance the more rapidly decelerating propellant material.

Inspection of the high-speed photographs revealed no evidence of reaction in the debris bubble. Other evidence of "cold" propellant debris included successful entrapment of the debris in a box of cotton batting. Ignition in this situation is unlikely because breakup involves mostly tensile processes (Reference 3), and other studies indicate that impact-induced ignition of this propellant is due to shear deformation (Reference 4).

Debris Bubble Impact Process (Unconfined Air Gap). In Test 2, the second propellant layer and second steel plate were included. The air gap for this experiment (3.0 inches), was larger than that for most of the tests against the inert simulant (1.9 inches) so that in-bore processes could be observed over a longer time. As with the first test, the air gap between the two propellant layers was left open (no Plexiglas surround). Figure B-2 contains a series of high-speed photographs showing the impact process for this test.

Prior to impact with the second propellant layer (Frames 1 through 6), the penetration and reaction behavior were similar to those of Test 1. The first significant change occurred upon impact of the debris bubble with the second propellant layer (Frame 7), and involved ignition of propellant along the impact surface beginning at the point of initial contact. A sketch of the ignition process is shown in Figure 5.

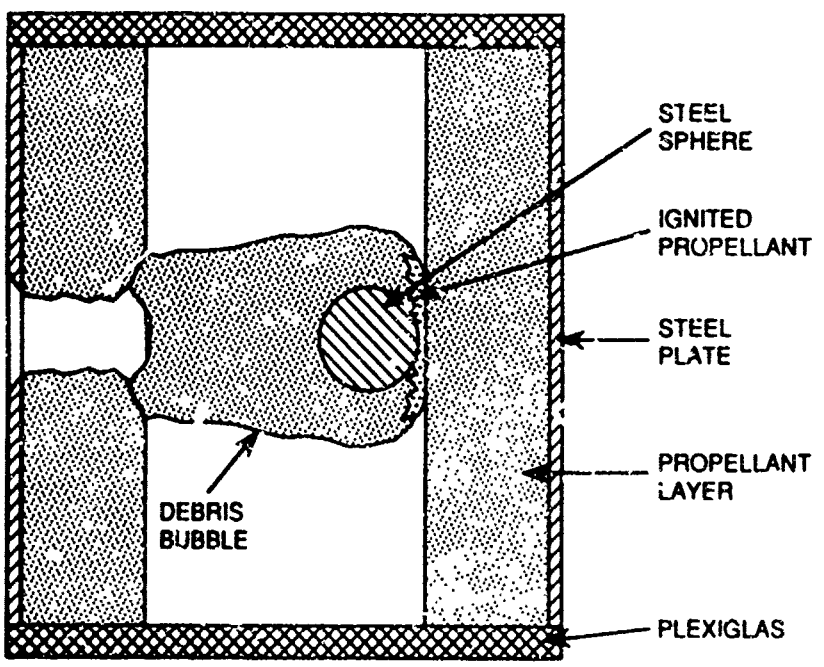

FIGURE 5. Sketch of Debris Bubble Ignition Process.

From the point of ignition, the reaction spread both laterally along the contact surface and back toward the first propellant layer (Frames 8 through 12). In front of the target, rearward-moving propellant ejecta, resulting from impact of the first propellant layer ignited after a period of time (Frame 11). After a much longer period of time (not shown), propellant debris resulting from perforation of the second propellant layer ignited to the rear of the target. Most of the propellant

material in this test was consumed. A slower speed video film of the test showed large pieces of burning propellant being thrown out from the test fixture.

Debris Bubble Impact Process (Confined Air Gap). Test 3 was a repeat of Test 2, but with the addition of a Plexiglas surround to provide some confinement for reaction enhancement. Figure B-3 is a sequence of high-speed photographs from this test. The maximum velocity of the debris bubble within the air gap was estimated at 2331 ft/s, while the terminal velocity of the projectile after complete penetration of the target was 1697 ft/s.

Ignition of the debris bubble occurred in Frame 6, at the same location as in Test 2. The reaction was more energetic and longer lasting; the Plexiglas cover shattered into many pieces; and, as in Test 2, most of the propellant was consumed.

Inspection of Frames 7 through 9 indicates that reaction occurred primarily in the region surrounding the debris bubble rather than in the bubble itself. This observation is interpreted to mean that reaction was primarily taking place in debris that had been deflected laterally along the second propellant layer and rearward at the Plexiglas surround. A sketch of a proposed flow/reaction pattern for the post-impact debris (assuming inelastic impacts) is shown in Figure 6.

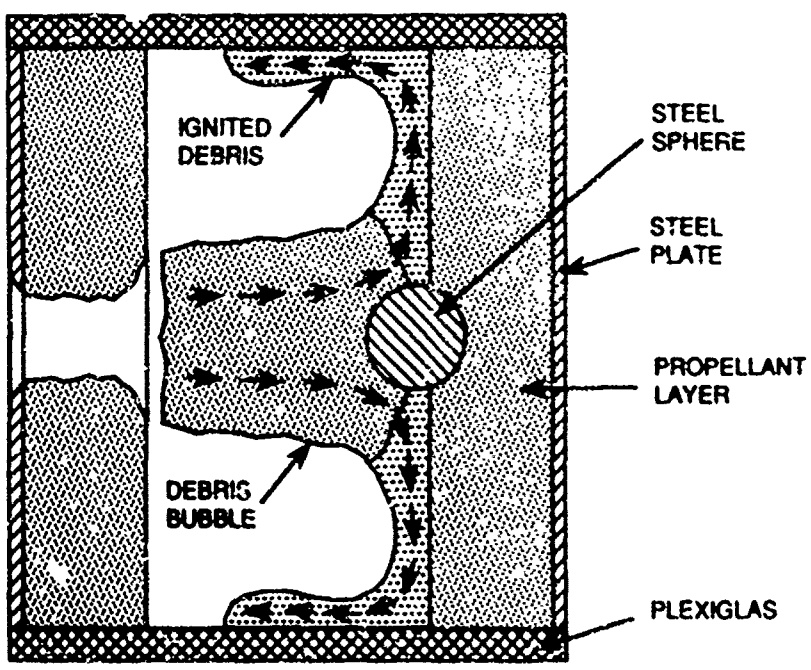

FIGURE 6. Sketch of Propellant Debris Flow/Reaction Patterns.

Air-Gap Influence on Reaction Process. A series of three tests were conducted to look at the influence of the air gap on ignition and burning processes. Plexiglas was used to enclose the sides of the target as in Test 3. Air gaps of 1.5, 3, and 7 inches were compared.

At the two smaller distances (1.5 and 3 inches), the projectile was still submerged within the debris bubble when the bubble struck the second propellant layer. It is possible, therefore, for propellant debris to be ignited by becoming compressed between the projectile and the second propellant layer during impact. Conversely, at the largest distance (7 inches), the projectile was clearly at the front of the debris bubble, which suggests that ignition by impacting projectile and propellant debris should occur more-or-less independently.

Propellant samples for Tests 4 through 11 and 13 were cut from different parent material than those for Tests 1 through 3. Test 4 was a repeat of Test 3 to ensure that penetration and reaction processes were the same for both materials. A comparison of the results, in Figures B-3 and B-4, shows essentially no difference in the behavior for the two tests.

The reaction appeared to be more energetic when the air gap was reduced to 1.5 inches (Test 5). When the gap was increased to 7 inches (Test 6), there was a significant reduction in reaction intensity. The shape of the reaction zone (rearward-facing cone) was also quite different for a 7-inch gap (Figure B-6, Frames 10 through 12), although it still appeared to be associated with debris from the first layer. In this case, however, the impacting debris cloud formed a large number of microcraters on the surface of the second layer. Burning ejecta from these craters traveled rearward through the interior of the debris bubble as seen in Figure 7, rather than around the bubble as seen in Figure 6. The ejecta system in Figure 7 should occur to some degree in all of the impacts. For small air gaps, however, reactions involving this system are probably obscured by the more dominant outward-flowing debris system.

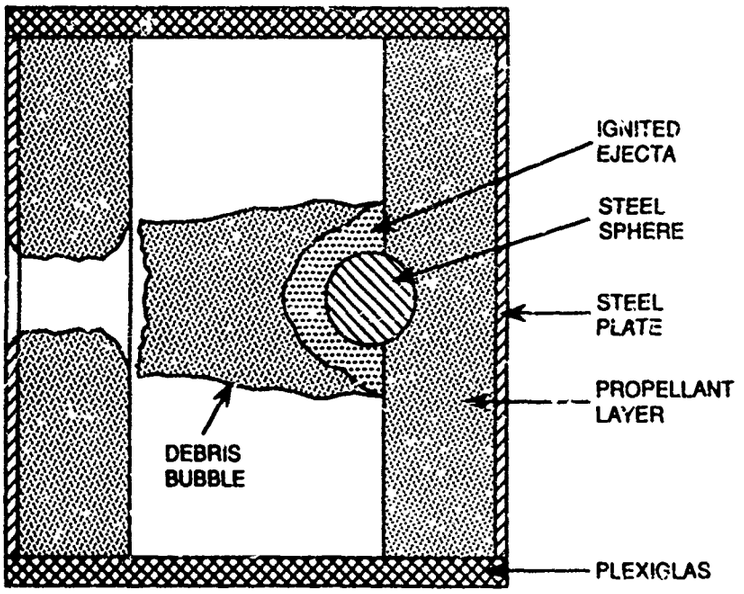

FIGURE 7. Sketch of Crater Ejecta Reaction Pattern.

Debris Cloud Ignition Studies. Results of the first six tests showed that reaction started at the point of initial contact between the debris bubble and the second propellant layer. The limited resolution of the high-speed photographs prevented a detailed study of the ignition process in this area. It would appear, however, that the primary ignition mechanism was associated with the impact of the projectile and might involve sandwiching of propellant debris between the projectile and the second propellant layer. There was no evidence of ignition of individual propellant particles impacting the second layer.

To examine the ignition and burning process in more detail, a series of five targets containing combinations of live and inert propellant were tested. In three of the tests (Tests 7 through 9), the second propellant layer was replaced by inert simulant. The air gaps for these tests were 3, 1.5, and 7 inches, respectively. In the other two tests (Tests 10 and 11), the first layer was replaced by simulant. The air gaps for these tests were 3 and 7 inches, respectively.

Figures B-5 and B-8 compare the reactions for targets with the same air gap (1.5 inches) and either (a) two live propellant layers (Test 5) or (b) first layer live and second layer inert (Test 8). Initially, the reactions were similar. However, at later times, the reaction in the target with two live propellant layers appeared more energetic. Similar differences in reaction intensity occurred for air gaps of 3 inches

(Tests 4 and 7) and 7 inches (Tests 6 and 9). These differences are probably due to the larger amount of "ignitable" material available in the live-live tests.

For tests where the first propellant layer was replaced by simulant (Tests 10 and 11), no sustained reaction occurred. There was only a brief flash when the debris bubble impacted the second layer (Figure B-10, Frame 7, for example). Apparently, sustained reaction along the surface of the second propellant layer is due to combustion of debris from the first layer bubble. This observation provides additional support for the reaction model proposed in Figure 6.

Although the sustained reaction changed when one of the propellant layers was replaced by simulant, the initial ignition flash did not. In other words, the "intensity" of the ignition light and the shape of the light envelope were similar for Tests 3 through 11. All of the ignition light envelopes tended to be irregular in outline. This suggests that ignition could occur in a number of separate sites around the initial impact point. The existence of a number of separate ignition sites is usually interpreted in terms of a "hot spot" ignition model involving some kind of localized heating process (e.g., adiabatic shearing, void collapse, or fracture of energetic particles) (References 4 and 5). Jetting processes along the interface between the projectile and the second layer may also be important.

A target with two inert propellant layers was used (Test 12) to generate a light signature under completely inert conditions. The result, shown in Figure B-12, was inconclusive. The first frame showed that contact between the debris bubble and the second layer occurred too late to view the impact flash at its maximum. Even so, the light appeared to be much dimmer than for impacts involving energetic material.

Crater Ejecta Ignition Study. The dominant reaction in targets with a large air gap appears to be associated with debris cloud material ejected from microcraters on the surface of the layer (Figure 7). To study impact cratering effects caused by projectile and plate fragment impacts alone, Test 13 was conducted on a target with a first steel plate, but no first propellant layer. The velocity in the air gap was higher in the absence of the first propellant layer (approximately 3400 ft/s versus 2400 ft/s). Hence, the results of this test are not directly comparable to the other tests. Results for Test 13 are shown in Figure B-13. They indicate a substantial increase in reaction compared to the test with an inert first layer (Test 11). This is consistent with the higher impact velocity of the projectile and plate fragments against the second layer.

Comparison With Prior Tests Using Inert Simulant. Prior experiments showed that projectile perforation of an inert propellant layer resulted

in a bubble of propellant debris being ejected from the rear surface (Reference 3). These experiments also showed that the amount of breakup of the debris could be reduced if the breakup process was interrupted as a result of impact with a second propellant layer spaced a short distance away. Interruption of the breakup process resulted in formation of long strips of partially fractured, "shredded" material.

The present experiments show that ignition of propellant ejecta within the bore is a major cause of BVR. These experiments also show that reaction intensity depends not only on the amount of burn surface created but also on the separation between the particles. The most energetic reactions occur at relatively small air gaps where the debris cloud is compressed as it collides with the second propellant layer and then flows outward, fluid-like, along the surface. Conversely, the least energetic reactions occur at large air gaps where particle separation is large.

It is interesting to note that the most energetic reactions in the present experiments occur under conditions where interference by the second propellant layer produced "shredded" debris in the earlier inert tests. The fluid-like flow pattern for the post-impact debris depicted in Figure 6 is also found under these same conditions.

HEP-1 PROPELLANT

The amount of HEP-1 propellant available for testing consisted of one 1.4-inch- and four 0.5-inch-thick slabs of 6-inch-diameter material. As a result, only one test (Test 15) of a complete target system (using two layers of propellant) could be made. In addition, one test (Test 14) of a half-target (consisting of a cover plate and one layer of propellant) was also made to study debris bubble characteristics. The two tests, similar to Tests 3 and 1 for HTPB/AP propellant, allowed comparison of the two propellant types. To make the comparison as meaningful as possible, the 1.4-inch-thick piece of propellant was used as the first layer in the full target system, while two of the 0.5-inch pieces, sandwiched together, were used as the second layer, and also in the half-target system.

The results of the half-target test are shown in Figure B-14. Because of the reduced thickness of the propellant layer (and possibly its sandwiched construction), a comparison with the comparable test involving HTPB/AP is qualitative. The apparent reduction in opacity of the debris bubble, indicative of fewer particles, was probably caused by the reduced thickness of the initial layer. On the other hand, the absence of reaction in the bubble was probably not related to the initial thickness, but rather to fundamental deformation/fracture processes. As in

Test 1, propellant debris was successfully recovered in cotton batting, which confirmed that it was cold.

Results for the complete target system are shown in Figure B-15. Like the HTPB/AP propellant, reaction occurred upon impact with the second propellant layer, although it was less energetic. Essentially all of the propellant was recovered (mostly in a few large pieces) after the test. The Plexiglas surround was blown apart during the test, although it did not shatter as in the test with HTPB/AP (Test 3).

HEP-2 PROPELLANT

The main purpose of this particular set of experiments was to examine the possibility of a delayed detonation (XDT) being initiated by the impact of a debris bubble composed of high-energy propellant. Studies involving the impact of cylindrical specimens of propellant material on steel barriers (Reference 2) have shown that sensitivity to XDT varies directly with the amount of damage suffered by the propellant during impact (a function of impact velocity) and also with the size of the sample. It appeared that the best way to trigger a XDT reaction using a planar motor configuration would be to produce the largest, highest-velocity debris bubble possible and then vary its characteristics (i.e., the amount of ejected mass, degree of damage, and particle sizes) by changing the width of the air gap until threshold conditions for XDT were met.

HEP-2 samples were all 3 by 4.5 by 1.5 inches. The lesser lateral dimension (3 inches) is about the same as the diameter of the crater produced in inert simulant under the same impact conditions and for a 1.9-inch air gap (Reference 3). It was felt that this was sufficiently large to avoid edge effects (except, possibly, for large air gaps).

Two kinds of experiments were conducted with HEP-2. Six tests (Tests 16 through 21) were conducted on targets containing only live material. The air gap was varied between 0.25 and 3.0 inches. In addition, two tests (Tests 22 and 23) were conducted on targets with inert second layers (HTPB/AP simulant). Air gaps of 1.0 and 1.5 inches were used for these targets.

Detonation in Live HEP-2. For air gaps of 0.25 and 3.0 inches, the debris bubble ignited upon impact with the second propellant layer, but the ensuing reaction died out. For air gaps between 0.5 and 2.5 inches, however, detonation occurred after debris bubble ignition.

The time delay between debris bubble impact and detonation changed with the width of the air gap, as shown in Figure 8, and also in Figures B-18 and B-20. For example, with a 2-inch air gap (Figure B-18), detonation occurred immediately after impact (Frames 8 and 9), while with a 0.5-inch air gap (Figure B-20), detonation occurred 6 frames after impact (Frames 4 through 10), and after complete perforation of the target (Frame 9). Detonation is indicated by gross overexposure and almost complete loss of detail in the remaining frames of the sequence.

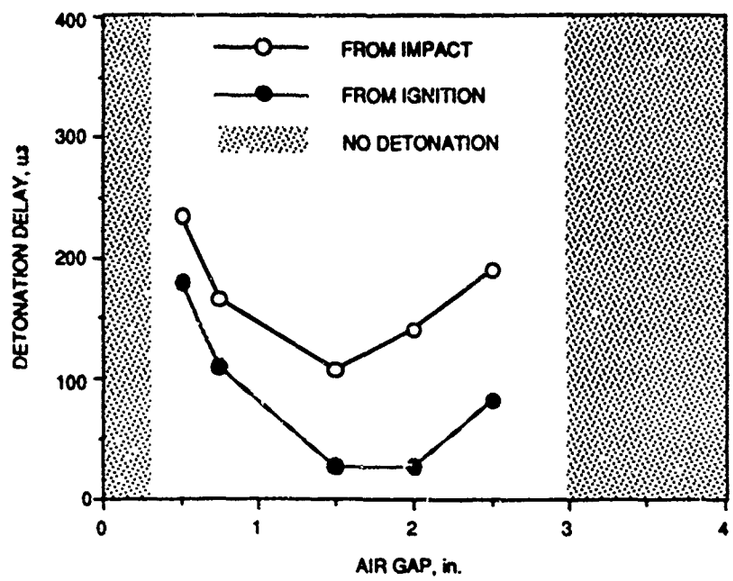

FIGURE 8. Detonation Delay Times for HEP-2 Propellant (Tests 16 Through 22).

Based on the delay time between impact and detonation, all detonations were classified as XDT reactions. For the test with the 2.0-inch air gap (Figure 18), detonation occurred less than 30 microseconds (one frame) after debris cloud impact. From the projected film (but not from the still frames in Appendix B), it can be seen that the second propellant layer detonated sympathetically approximately 2 frames (60 microseconds) after the first layer. This indicates that a detonation front must have traveled back through the incoming debris bubble to the first layer, as sketched in Figure 9.

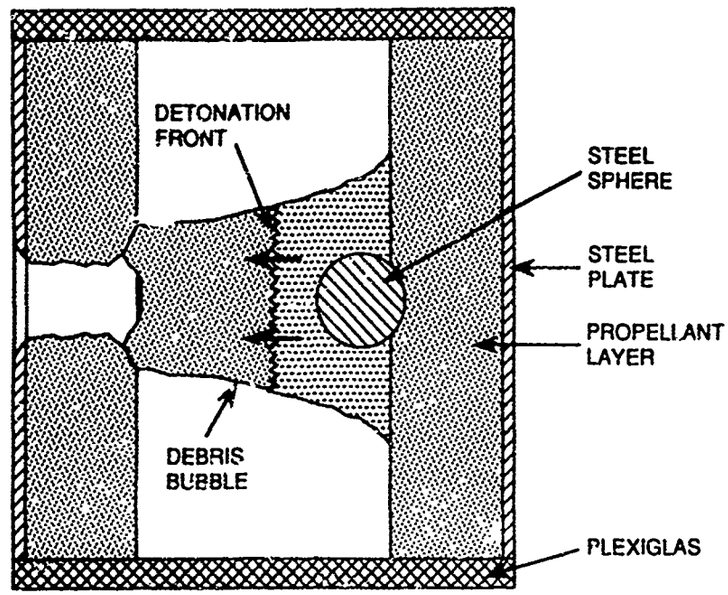

FIGURE 9. Sketch of XDT Reaction Process.

For the test with the 2.5-inch air gap (Test 17, Figure B-17), the second propellant layer did not detonate, although the first layer clearly did. Apparently, this air gap is sufficiently wide to prevent sympathetic detonation. The time delay for detonation also increased at this air gap beyond a value attributable to the increased width alone. The reason for this large delay is not known.

Effect of Inert Second Layer. The test involving a target with an inert second layer and with a 1.5-inch air gap (Test 22) resulted in an XDT reaction. Detonation occurred immediately after the debris bubble impacted the second propellant layer. This result is similar to that observed for a 2-inch gap with both layers live. The test involving a target with a 1.0-inch air gap (Test 23) resulted in a transient burning reaction within the air gap that did not transition to detonation.

The concept shown in Figure 9 may not apply for delayed detonations occurring in very small air gaps. The lack of detonation in the 1.0-inch air gap test indicates that the second propellant layer is involved in initiating XDT for small air gaps. An inspection of the impacted surface of the second propellant (simulant) layer in Test 23 showed considerable cratering in the center of the impact area. Similar cratering was also noticed in the same area for Test 12. Thus, cratering of the second layer might become a major influence at small air gaps.

CONCLUSIONS

1. Through the use of a planar rocket motor model, considerable qualitative information can be obtained regarding BVR phenomena at an inner bore. The planar rocket motor model thus becomes a useful research tool for examining inner bore reaction phenomena.

2. Debris bubble formation and material breakup at the rear of a propellant layer appear consistent with results of prior ballistic tests with inert material.

3. The cloud of debris ejected from the rear of the first propellant layer remains essentially cold (unreacted) unless the cloud contacts a second propellant layer. If a second layer is not present, the cloud does not react.

4. Reaction is initiated when the projectile strikes the second layer. Reaction does not appear to be caused by propellant debris striking the second layer.

5. With HTPB/AP propellant, burning occurs for a range of air gap spacings. Flame from the ignition point on the second layer reaches the first layer either by means of flow around inside of the box or, possibly, by means of a burning cloud of material from the second layer projected back inside the cloud from the first layer.

6. With the HEP-2 propellant, a delayed detonation (XDT) occurs over a range of air gap spacings. A detonation front appears to travel backward through the debris cloud toward the first propellant layer. When it reaches the first layer, this layer detonates. The second layer then detonates sympathetically.

RECOMMENDATIONS

1. Additional parametric studies should be conducted on these same propellant materials to look at the influence that other test variables such as projectile shape, impact velocity, web thickness/geometry, case materials, and confinement have on BVR processes.

2. Tests should be conducted using different propellants. This is necessary in order to (a) build a more comprehensive database, (b) establish the validity of reaction models discovered so far, and (c) determine sensitivity limits (error bars) for the test procedure.

3. The relationship between the reaction events occurring in planar motor tests and those occurring in actual motors should be determined. In particular, the effects of curvature and confinement must be assessed. This might be accomplished by conducting tests with a cylindrical motor section and photographing axially down the bore.

4. The planar rocket motor model may have potential for use as a screening test for propellant sensitivity. This would require that a suitable burning debris velocity or propagation limit be found that could be equated to reaction violence. These tests would be relatively inexpensive and easy to perform. A planar motor model composed of plates and propellant slabs is easier to fabricate than a cylindrical model. Only a high-speed camera is required for instrumentation. Alignment (firing to hit the center of the bore) is not critical.

5. The test procedure should be refined and improved. As discussed in previous sections, the results obtained so far have been uneven because of backlighting problems; transient light effects; nonuniform propellant dimensions, shapes, and surface finishes; and nonstandard target fabrication procedures. Faster camera speeds would also allow for more accurate evaluation of results.

REFERENCES

1. Graham, K. J., R. G. S. Sewell, and J. K. Pringle. "An Event Tree Model for the Fragment Initiation of Cased Explosives and Propellants," *Second JANNAF Propulsion Systems Hazards Subcommittee Meeting*, CPIA 356, Vol. 1 (April 1982), pp. 243-57.

2. Butcher, A. G., K. P. McCarty, R. L. Keefe, and E. J. Blommer. "A Summary of the Mechanisms of Delayed Detonation," *20th JANNAF Combustion Meeting*, CPIA Pub. 383, 1983.

3. Finnegan, S. A., J. C. Schulz, O. E. R. Heimdahl, J. K. Pringle, and A. J. Lindfors. "Impact-Induced Shredding Damage to Cased Elastomeric Propellant," *1989 JANNAF Propulsion System Hazards Subcommittee Meeting*, San Antonio, Texas, February 1989.

4. Ho, S. Y. "The Mechanism of Impact Ignition of Energetic Materials," *Ninth Symposium (International) on Detonation*, 1989, pp. 453-61.

5. Coffey, C. S. "Initiation of Explosive Crystals by Shock or Impact," *Ninth Symposium (International) on Detonation*, 1989, pp. 864-70.

Appendix A

DETAILED TABLE OF TEST CONFIGURATIONS AND RESULTS

Table A-1. Detailed Results for Planar Rocket Motor Model Test Firings.

Test	Impact configuration[a]					High-speed camera data					
						Measured velocities, ft/s				Detonation delay time, μs	
	1st steel plate[b]	1st propellant layer[c]	Air gap, in.	2nd propellant layer[c]	2nd steel plate[b]	Launch	Impact	Debris bubble[d]	Reaction front[e]	From impact	From ignition
1	Mild	HTPB	Infinite[f]	None	None	3898	2816	2611[g]/2473	...[h]	...[i]	...[i]
2	Hard	HTPB	3.0[f]	HTPB	Hard	3887	3845	2486	4395[j]	...[i]	...[i]
3	Hard	HTPB	3.0	HTPB	Hard	3919	3923	2331	4469[j]	...[i]	...[i]
4	Hard	HTPB	3.0	HTPB	Hard	3828	3742	2394	4785[j]	...[i]	...[i]
5	Hard	HTPB	1.5	HTPB	Hard	3776	3799	...[k]	...[k]	...[i]	...[i]
6	Hard	HTPB	7.0	HTPB	Hard	3890	3736	2596	2705[j]	...[i]	...[i]
7	Hard	HTPB	3.0	Inert	Hard	3761	3814	2499	...[k]	...[i]	...[i]
8	Hard	HTPB	1.5	Inert	Hard	3828	...[k]	...[k]	...[k]	...[i]	...[i]
9	Hard	HTPB	7.0	Inert	Hard	3790	3688	2610	3244[l]	...[i]	...[i]
10	Hard	Inert	3.0	HTPB	Hard	3827	3764	2427	...[k]	...[i]	...[i]
11	Hard	Inert	7.0	HTPB	Hard	3820	3645	2600	2749[l]	...[i]	...[i]
12	Hard	Inert	3.0	Inert	Hard	3897	3879	2417	2647[j,m]	...[i]	...[i]
13	Hard	None	3.0	HTPB	Hard	3832	3913	3323[n]	4235[l]	...[i]	...[i]
14	Mild	HEP-1[o]	Infinite[f]	None	None	3897	3715	3042[g]/2969	...[h]	...[i]	...[i]
15	Mild	HEP-1[p]	3.0	HEP-1[o]	Mild	3860	3898	2943	...[k]	...[i]	...[i]
16	Hard	HEP-2	3.0	HEP-2	Hard	4145	...[k]	2524	2770[j]	...[i]	...[i]
17	Hard	HEP-2	2.5	HEP-2	Hard	3968	3836	...[k]	...[k]	189	81

See footnotes at end of table.

Table A-1. (Contd.)

Test	Impact configuration[a]					High-speed camera data					
						Measured velocities, ft/s				Detonation delay time, μs	
	1st steel plate[b]	1st propellant layer[c]	Air gap, in.	2nd propellant layer[c]	2nd steel plate[b]	Launch	Impact	Debris bubble[d]	Reaction front[e]	From impact	From ignition
18	Hard	HEP-2	2.0	HEP-2	Hard	3892	. . .[k]	2295	. . .[k]	140	28
19	Hard	HEP-2	0.75	HEP-2	Hard	3832	3911	. . .[k]	. . .[k]	166	110
20	Hard	HEP-2	0.5	HEP-2	Hard	3770	3830	. . .[k]	. . .[k]	221	165
21	Hard	HEP-2	0.25	HEP-2	Hard	3875	3845	. . .[k]	. . .[k]	. . .[i]	. . .[i]
22	Hard	HEP-2	1.5	Inert	Hard	. . .[k]	3879	. . .[k]	. . .[k]	108	27
23	Hard	HEP-2	1.0	Inert	Hard	. . .[k]	4139	. . .[k]	. . .[k]	. . .[i]	. . .[i]

[a]Projectile = 3/4-inch mild steel sphere.
[b]Plate materials = 1/16-inch mild steel (mild) and 4130 steel (hard).
[c]1.5-inch thick (except as noted).
[d]Maximum velocity along centerline.
[e]After debris bubble impacts second propellant layer.
[f]Unconfined.
[g]Residual projectile velocity.
[h]No reaction front.
[i]No detonation.
[j]Along surface of second propellant layer.
[k]Velocity could not be measured.
[l]Normal to surface of second propellant layer.
[m]Velocity of inert material.
[n]Projectile and plate fragments only.
[o]1.0-inch thick.
[p]1.4-inch thick.

Appendix B

PHOTOGRAPHIC SEQUENCES FOR ALL TESTS

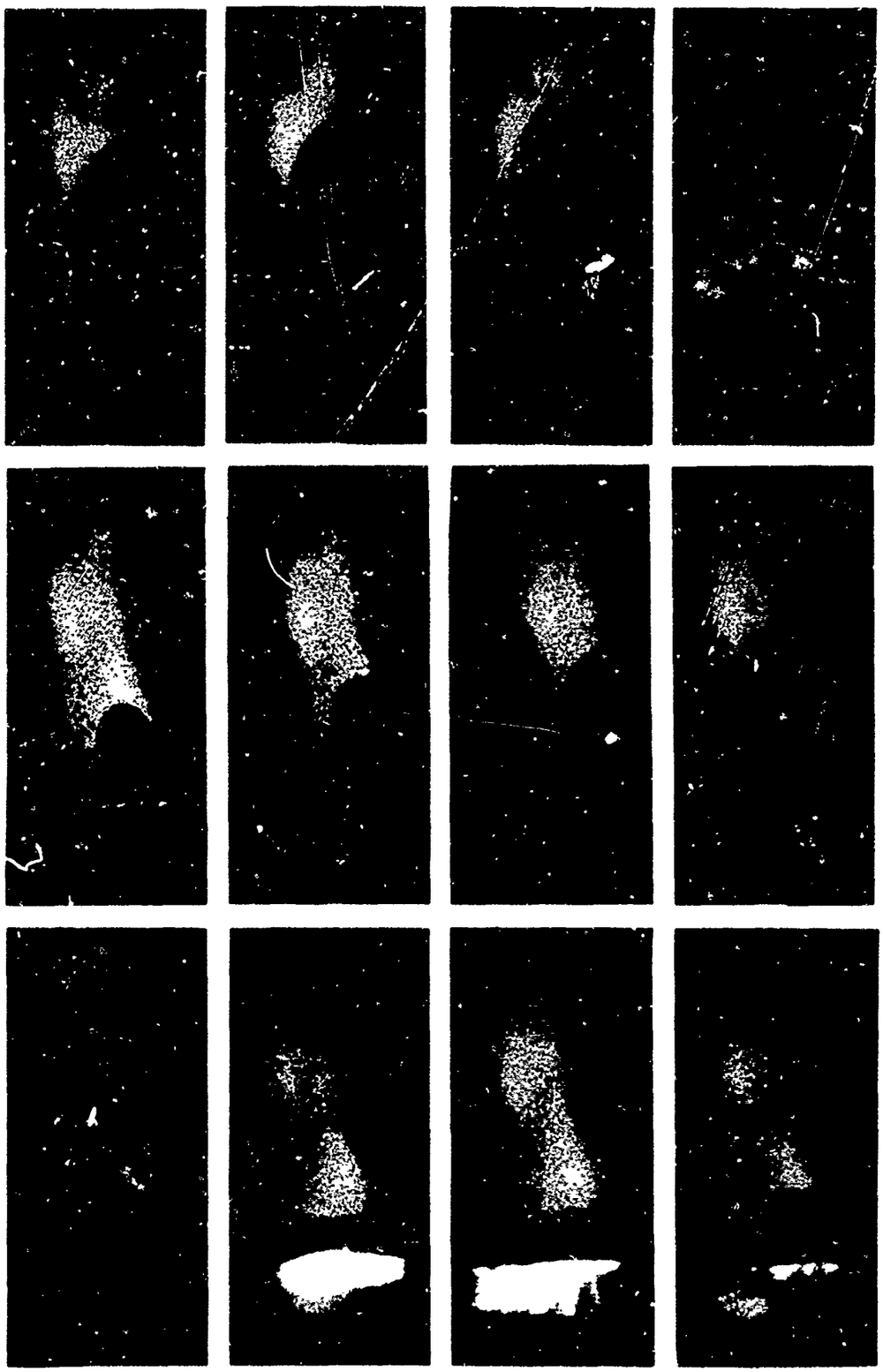

FIGURE B-1. Photographic Sequence for Test 1. (Mild steel, HTPB, infinite air gap, unconfined.)

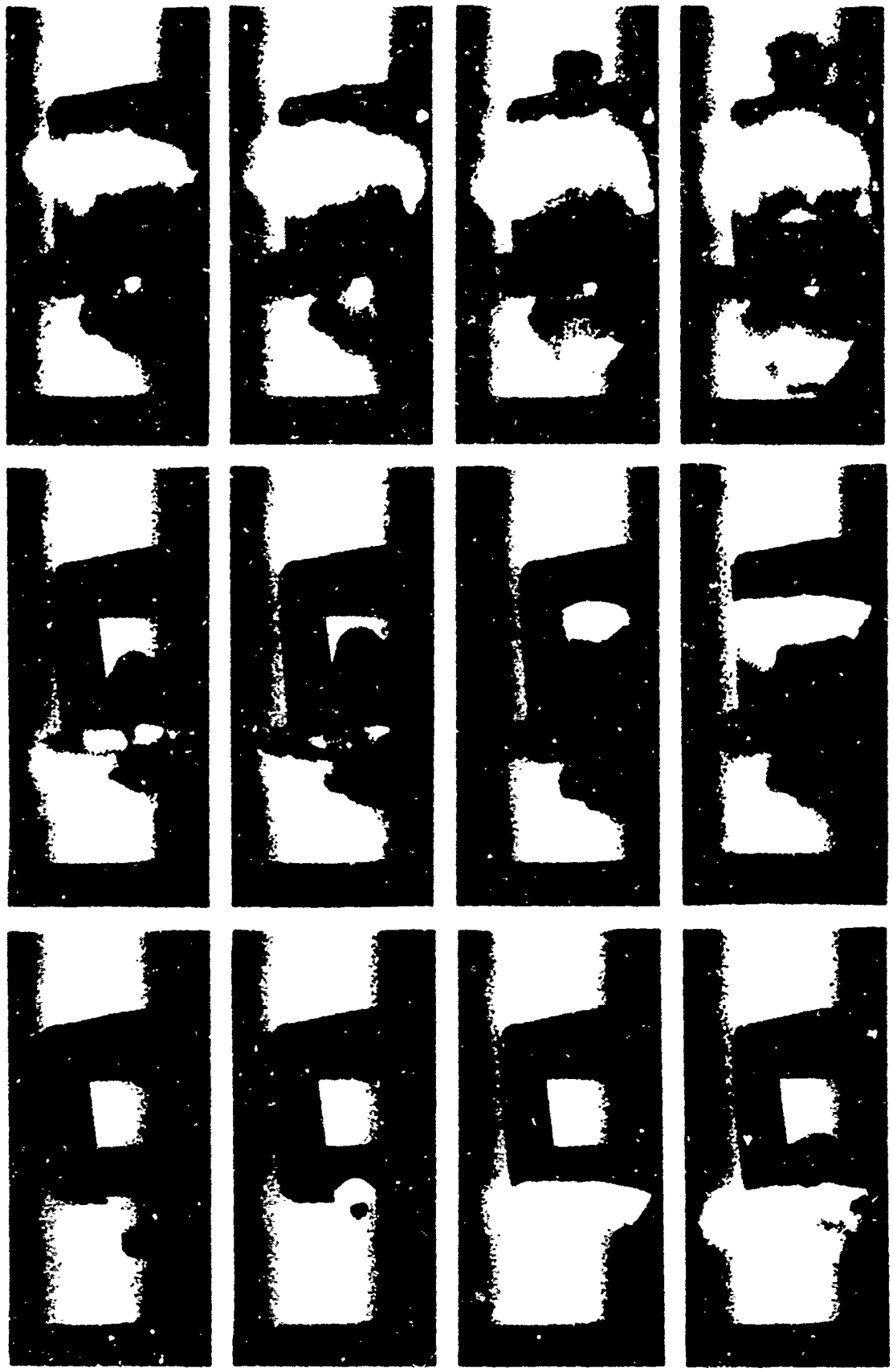

FIGURE B-2. Photographic Sequence for Test 2. (Hard steel, HTPB, 3.0-inch air gap, HTPB, hard steel, unconfined.)

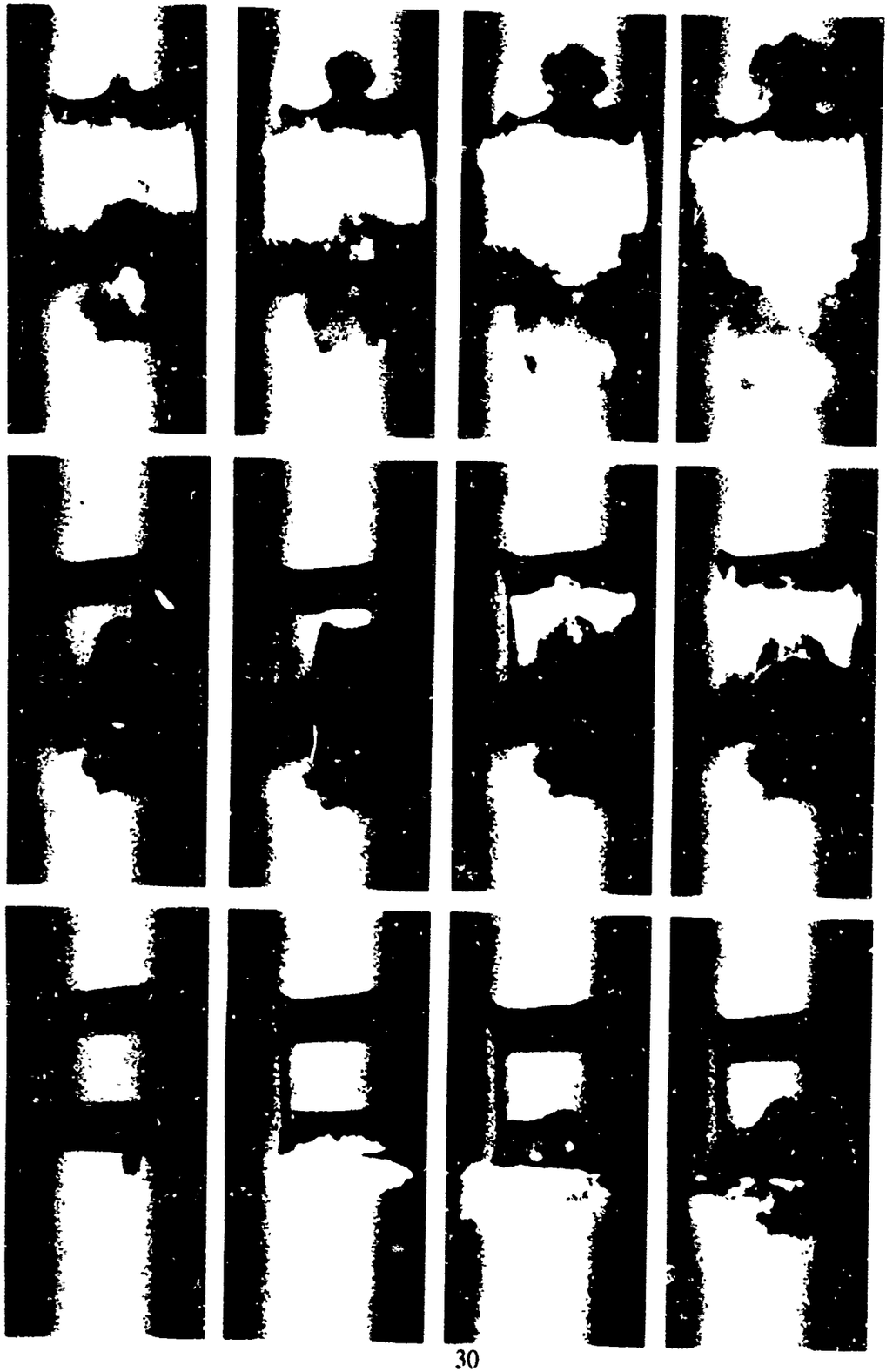

FIGURE B-3. Photographic Sequence for Test 3. (Hard steel, HTPB, 3.0-inch air gap, HTPB, hard steel.)

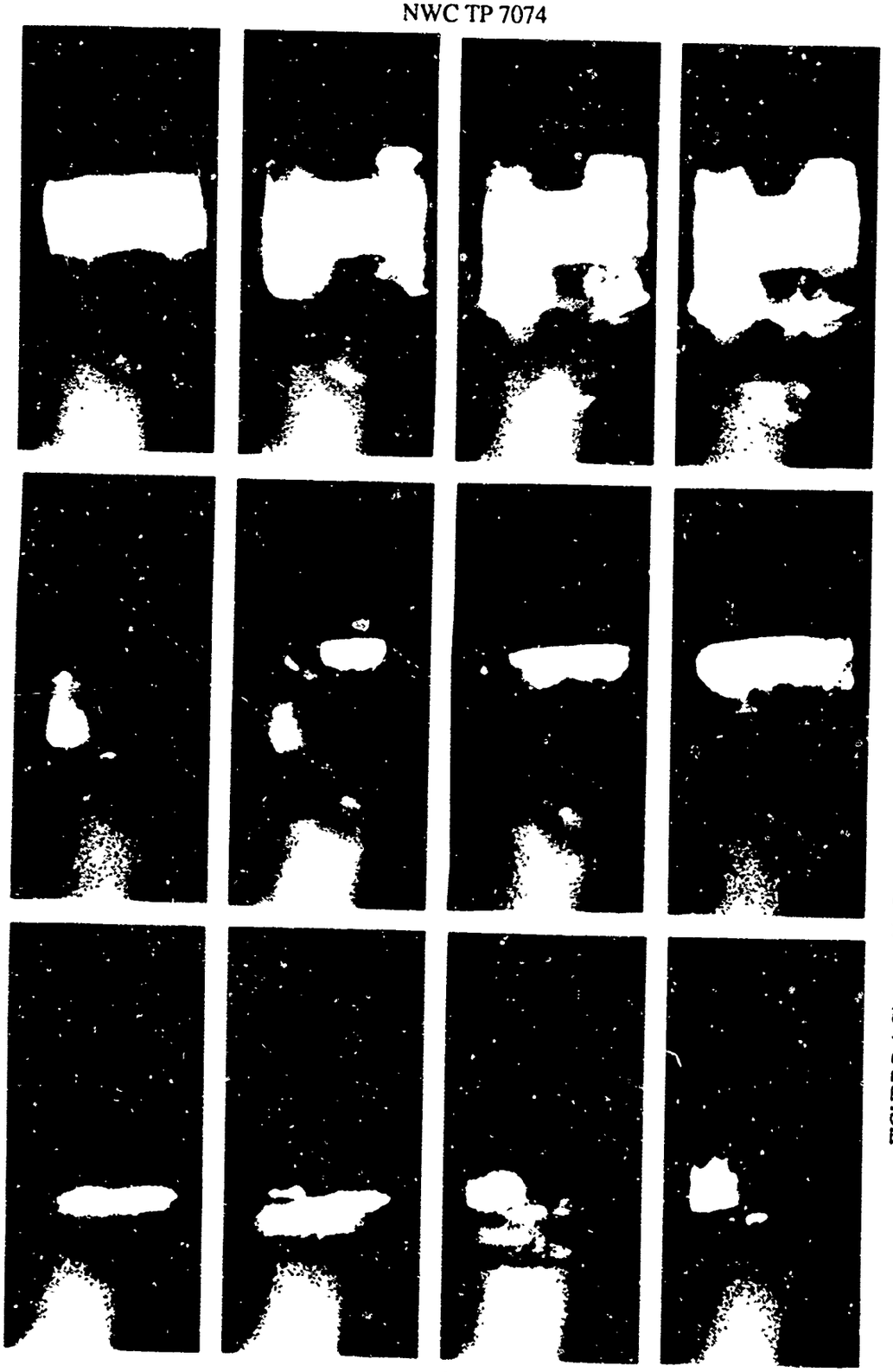

FIGURE B-4. Photographic Sequence for Test 4. (Hard steel, HTPB, 3.0-inch air gap, HTPB, hard steel.)

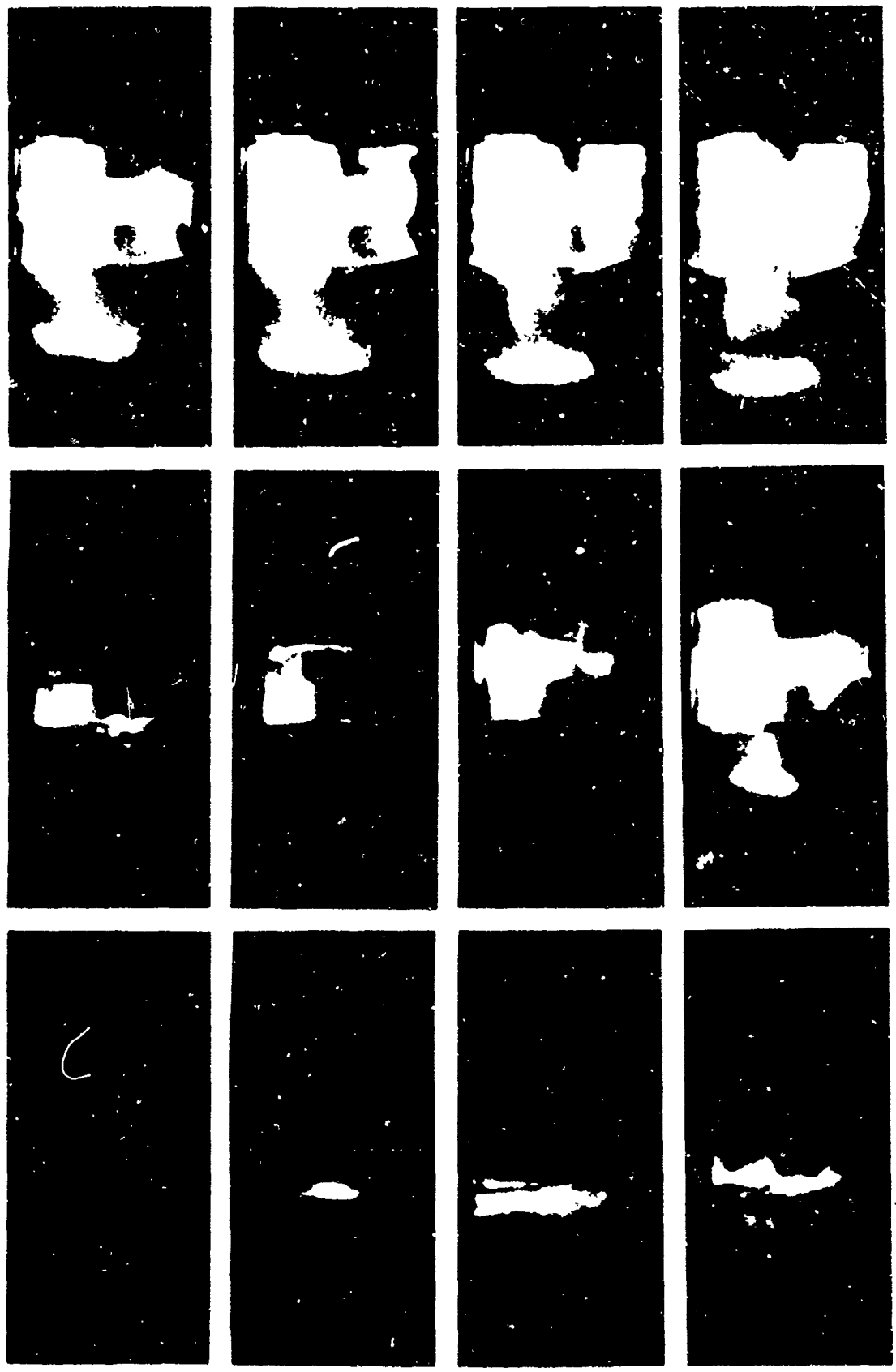

FIGURE B-5. Photographic Sequence for Test 5. (Hard steel, HTPD, 1.5-inch air gap, HTPB, hard steel.)

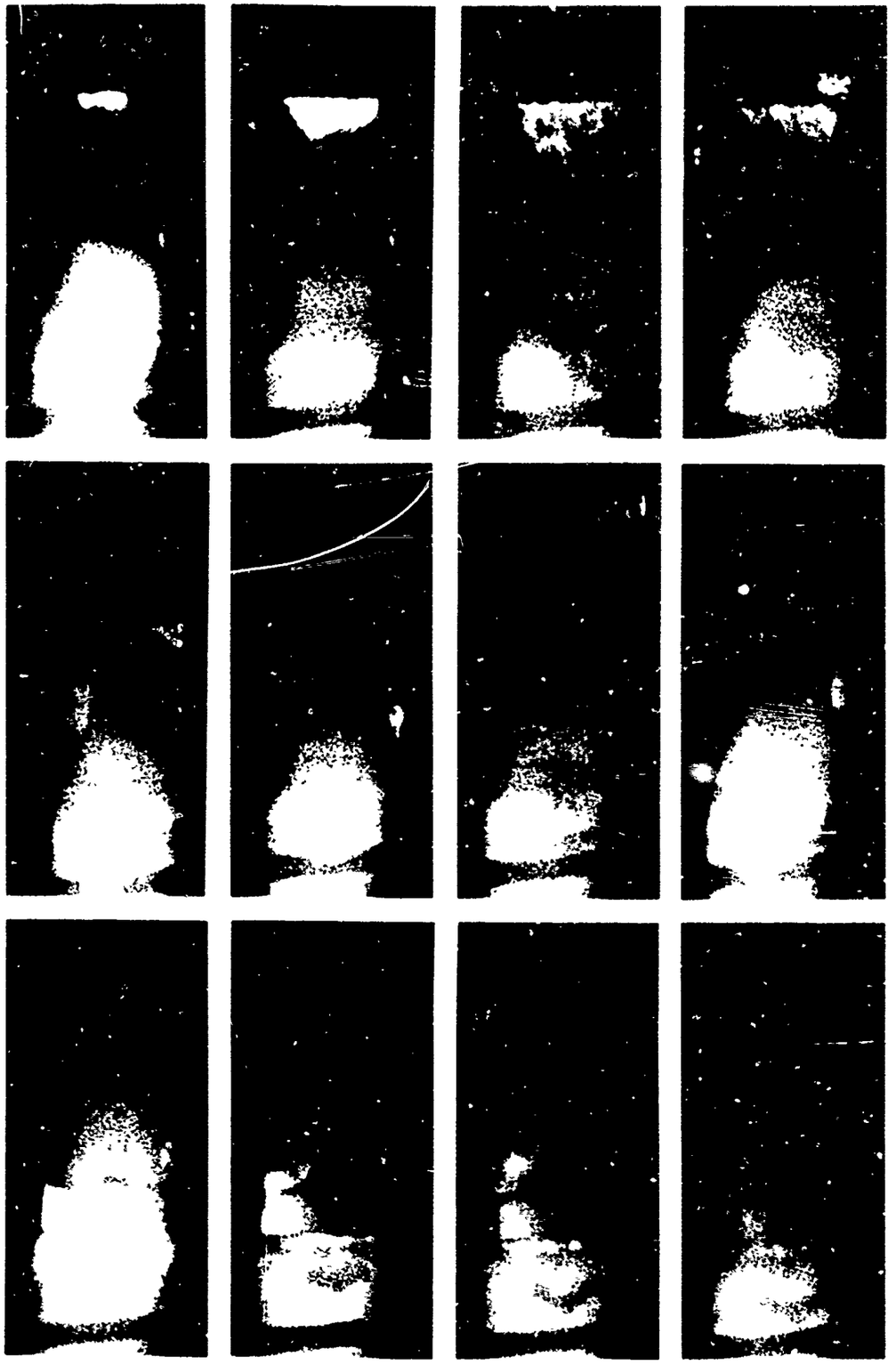

FIGURE B-6. Photographic Sequence for Test 6. (Hard steel, HTPB, 7.0-inch air gap, HTPB, hard steel.)

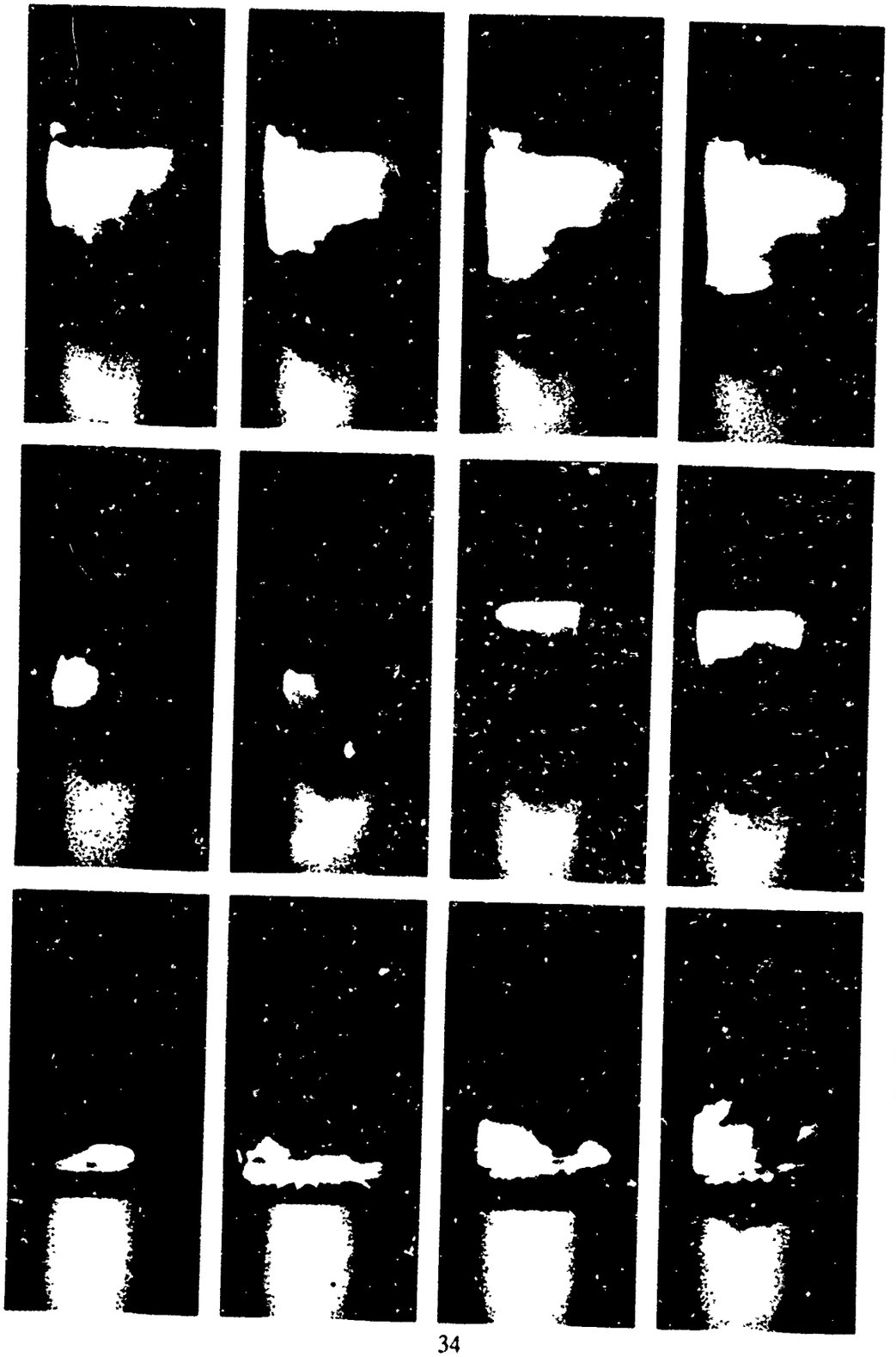

FIGURE B-7. Photographic Sequence for Test 7. (Hard steel, HTPB, 3.0-inch air gap, inert, hard steel.)

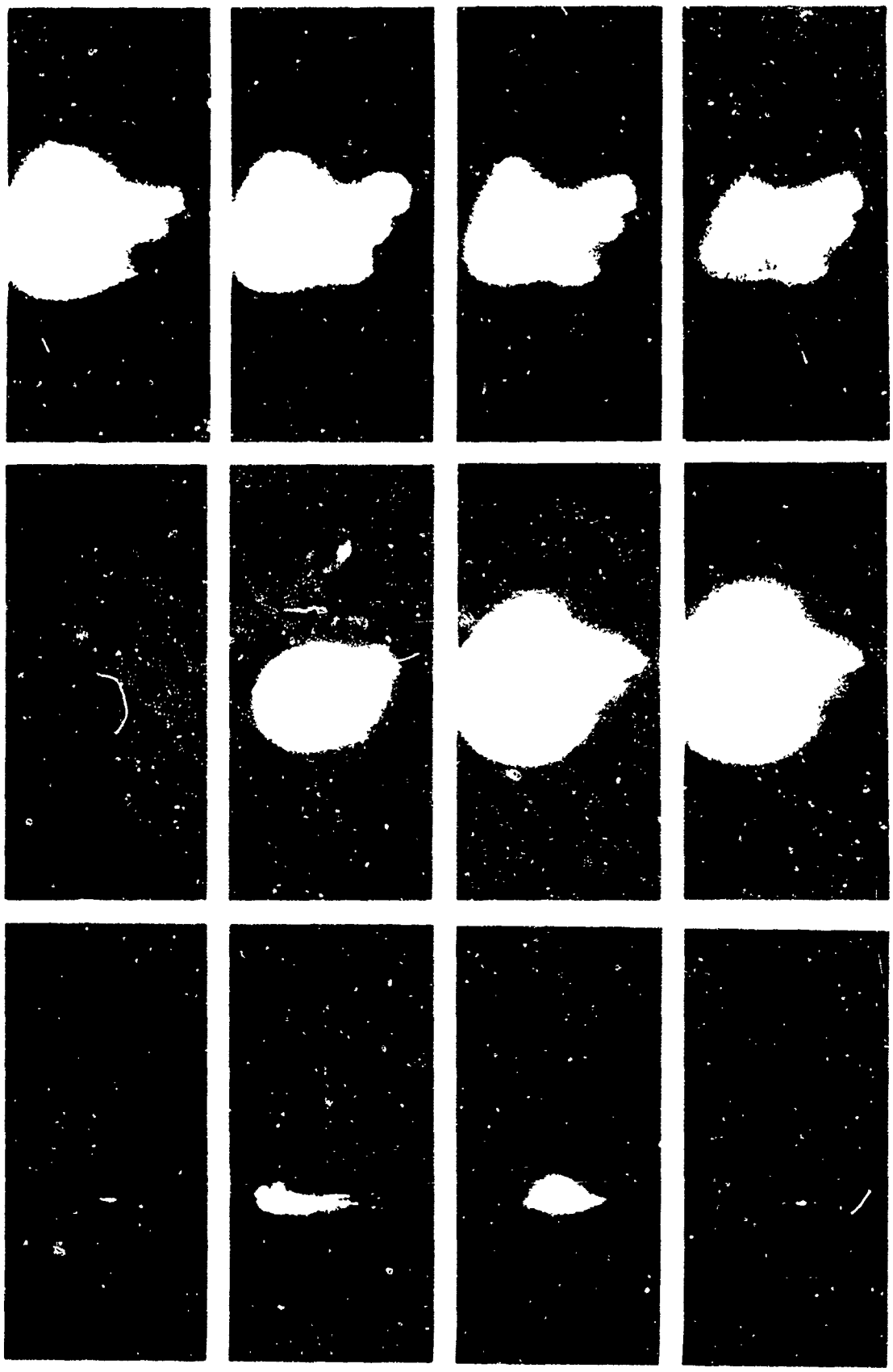

FIGURE B-8. Photographic Sequence for Test 8. (Hard steel, HTPB, 1.5-inch air gap, inert, hard steel.)

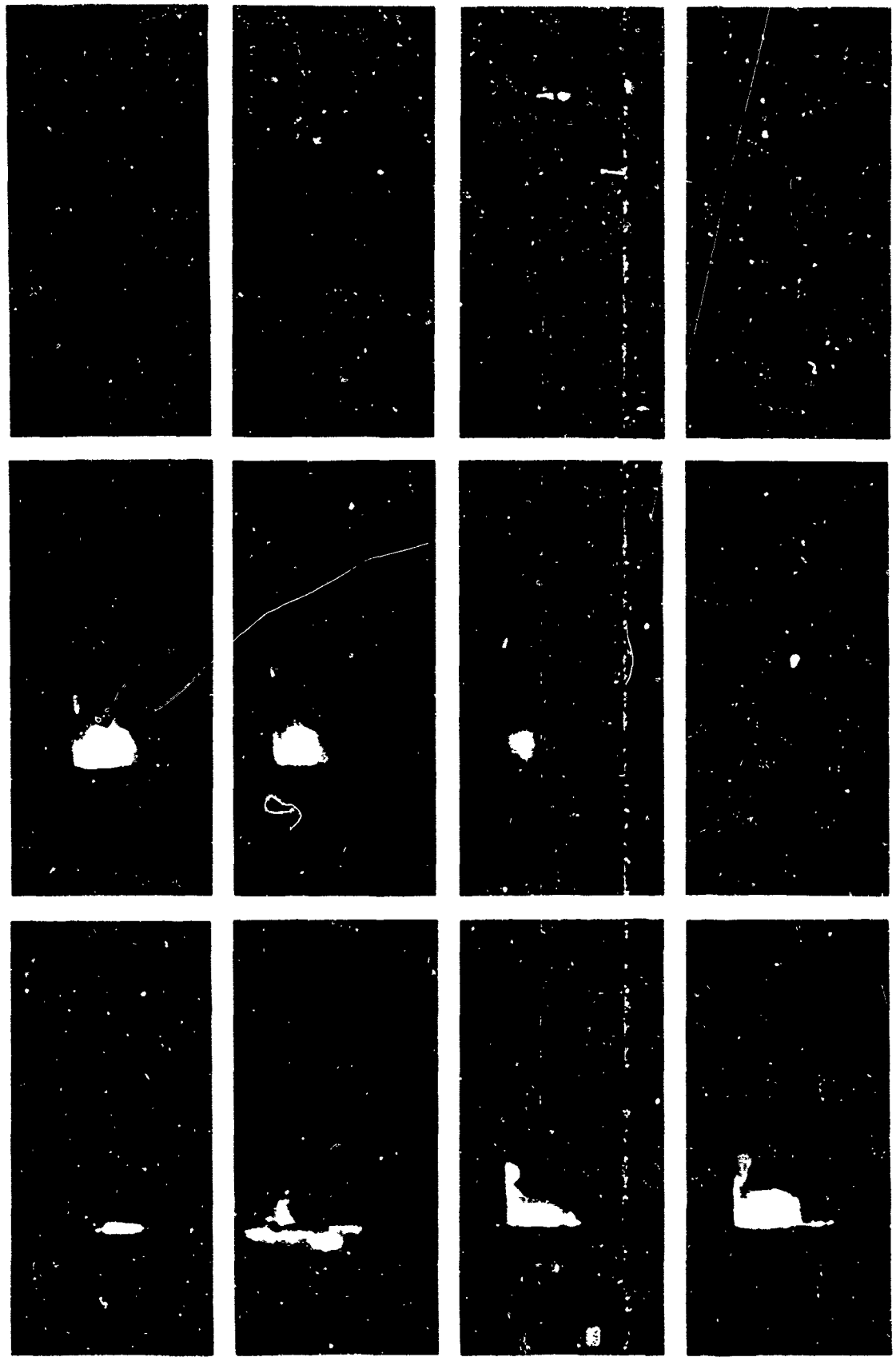

FIGURE B-9. Photographic Sequence for Test 9. (Hard steel, HTPB, 7.0-inch air gap, inert, hard steel.)

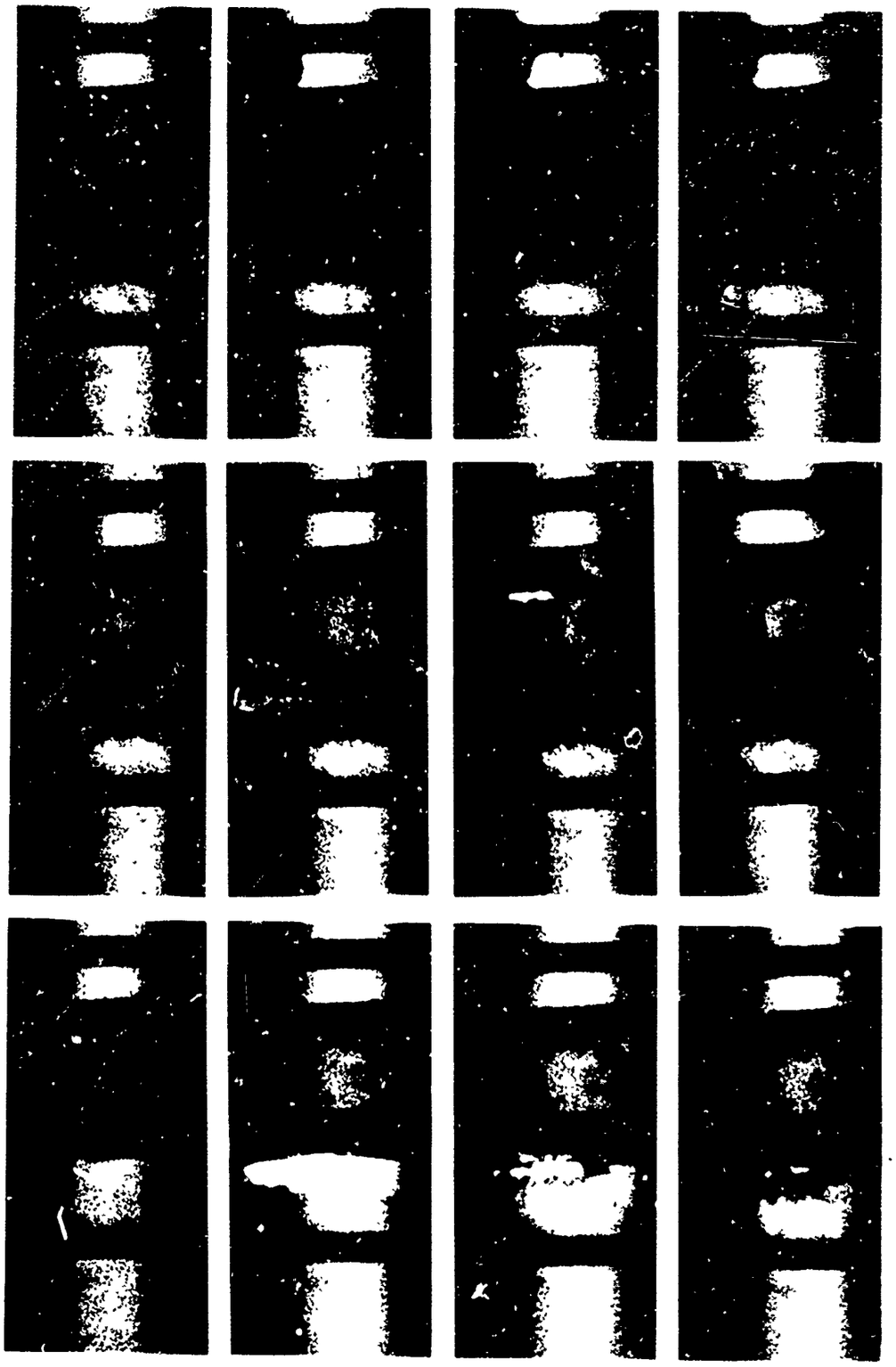

FIGURE B-10. Photographic Sequence for Test 10. (Hard steel, inert, 3.0-inch air gap, HTPB, hard steel.)

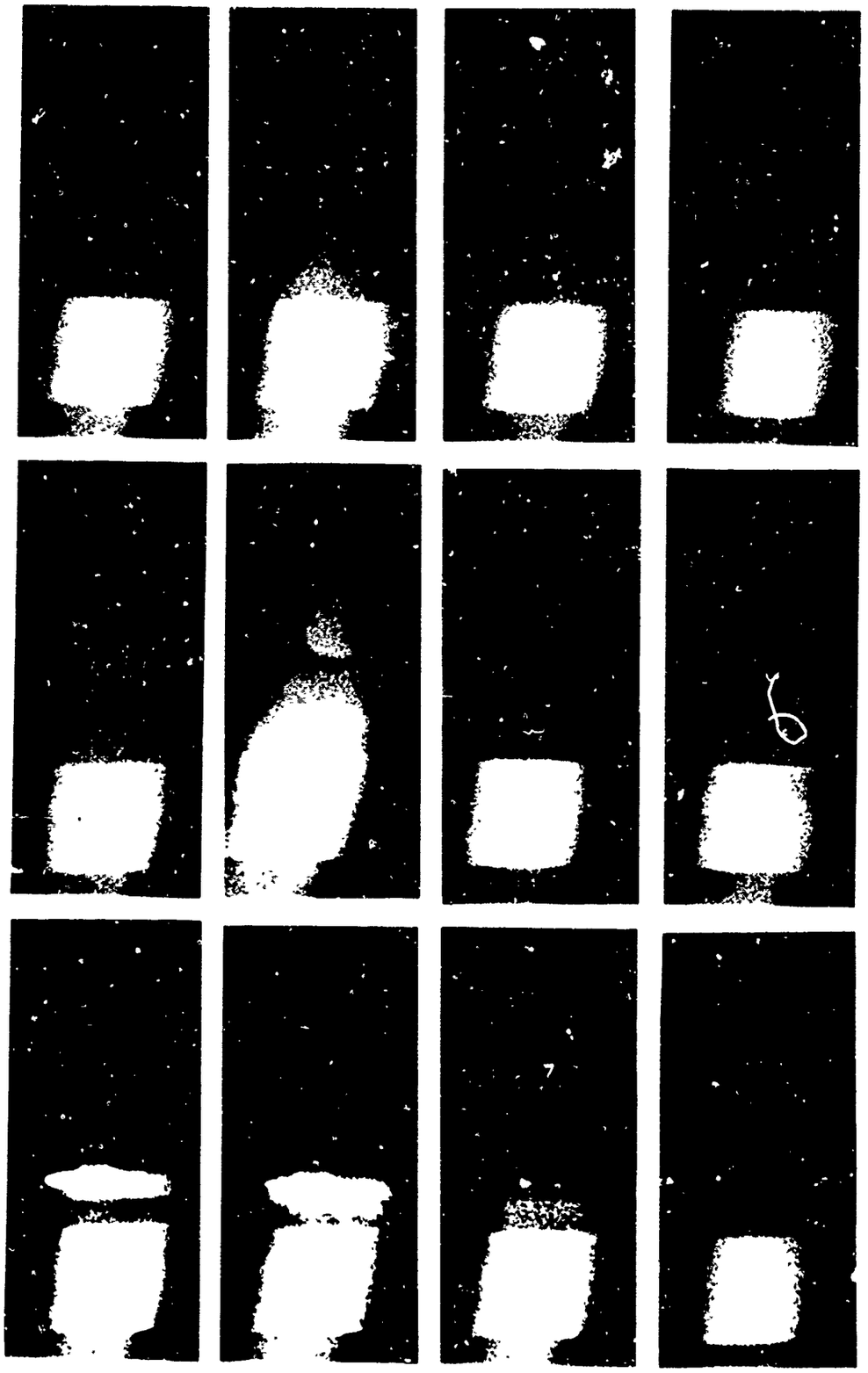

FIGURE B-11. Photographic Sequence for Test 11. (Hard steel, inert, 7.0-inch air gap, HTPB, hard steel.)

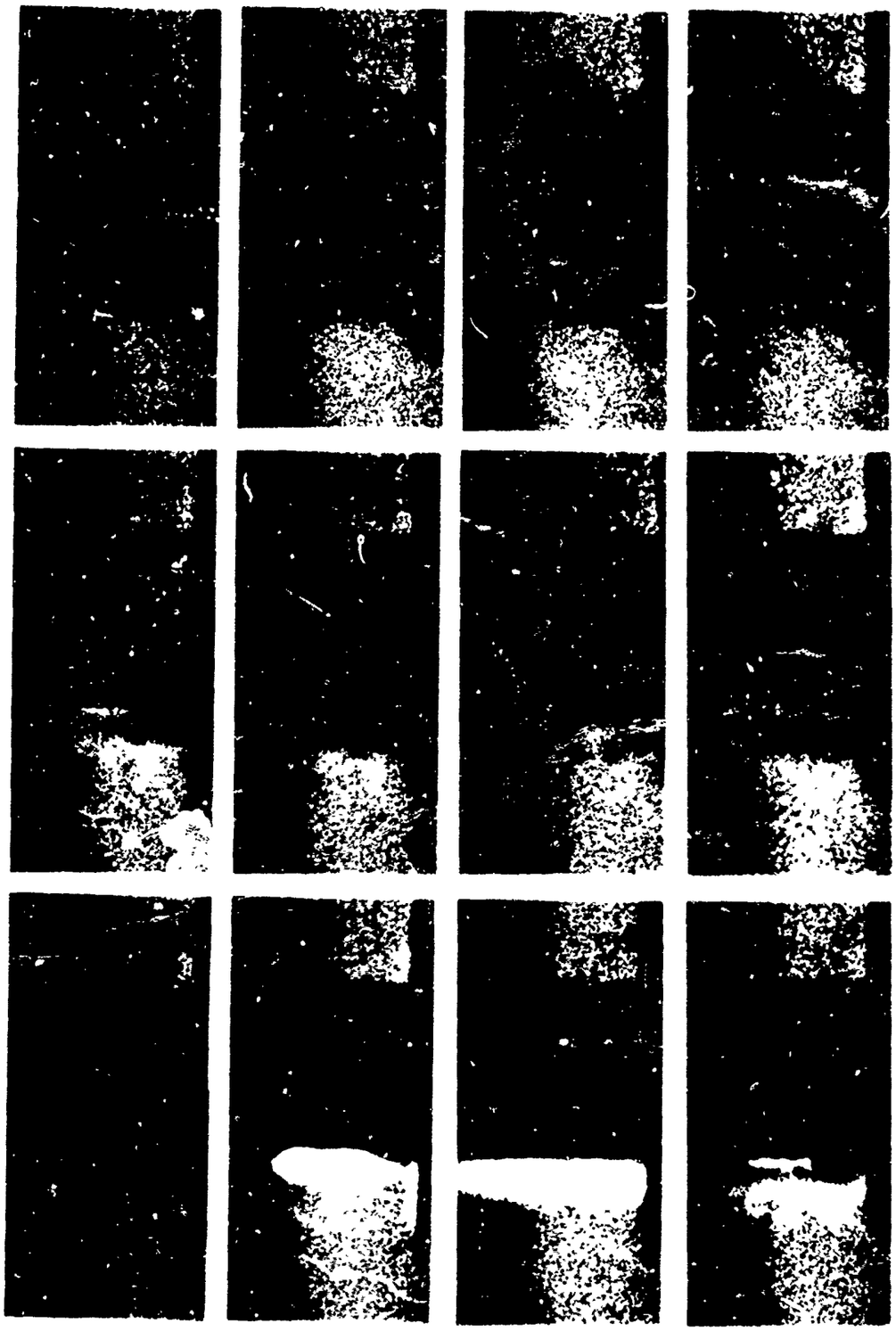

FIGURE B-12. Photographic Sequence for Test 12. (Hard steel, inert, 3.0-inch air gap, inert, hard steel.)

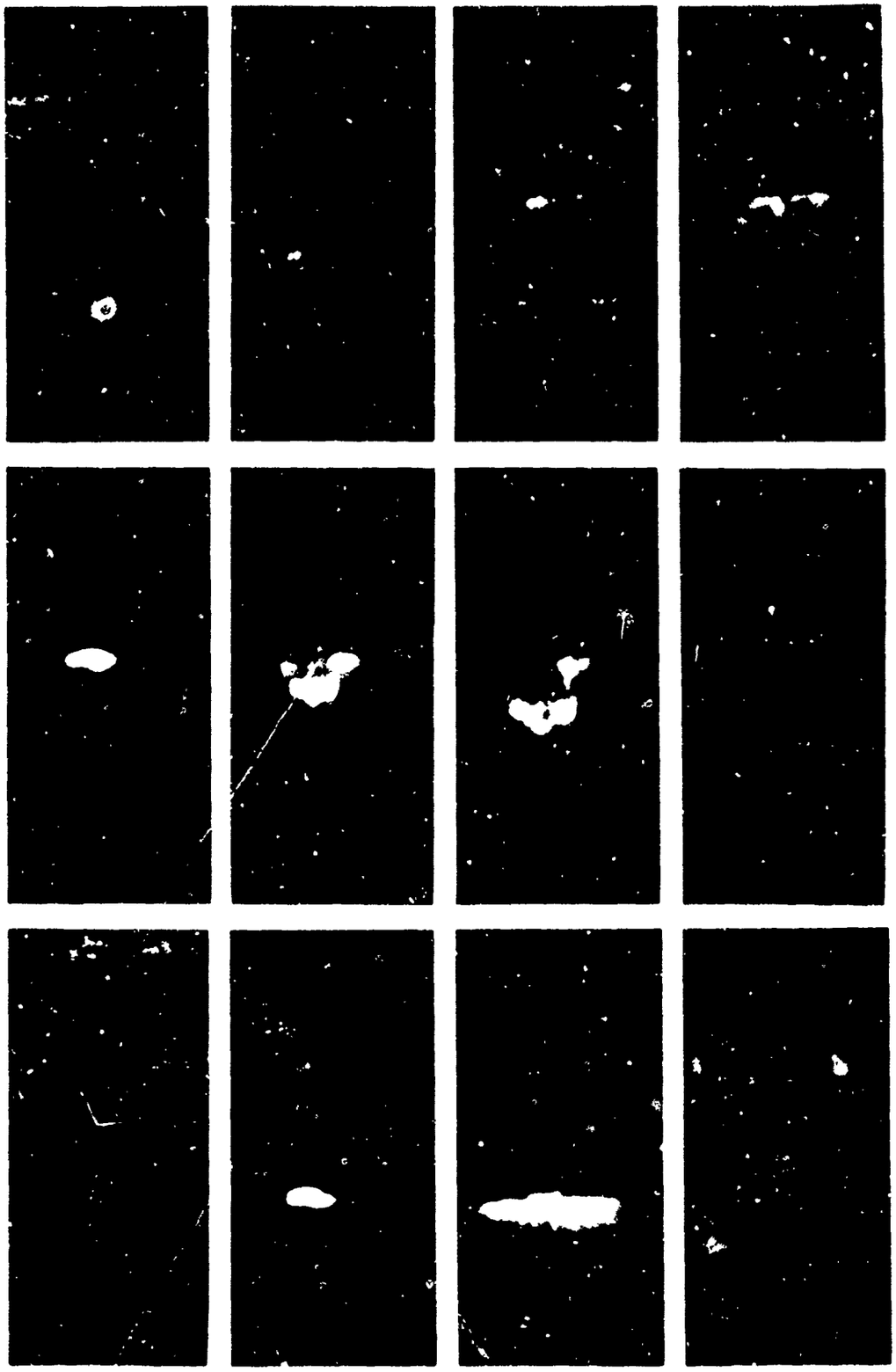

FIGURE B-13. Photographic Sequence for Test 13. (Hard steel, none, 3.0-inch air gap, HTPB, hard steel.)

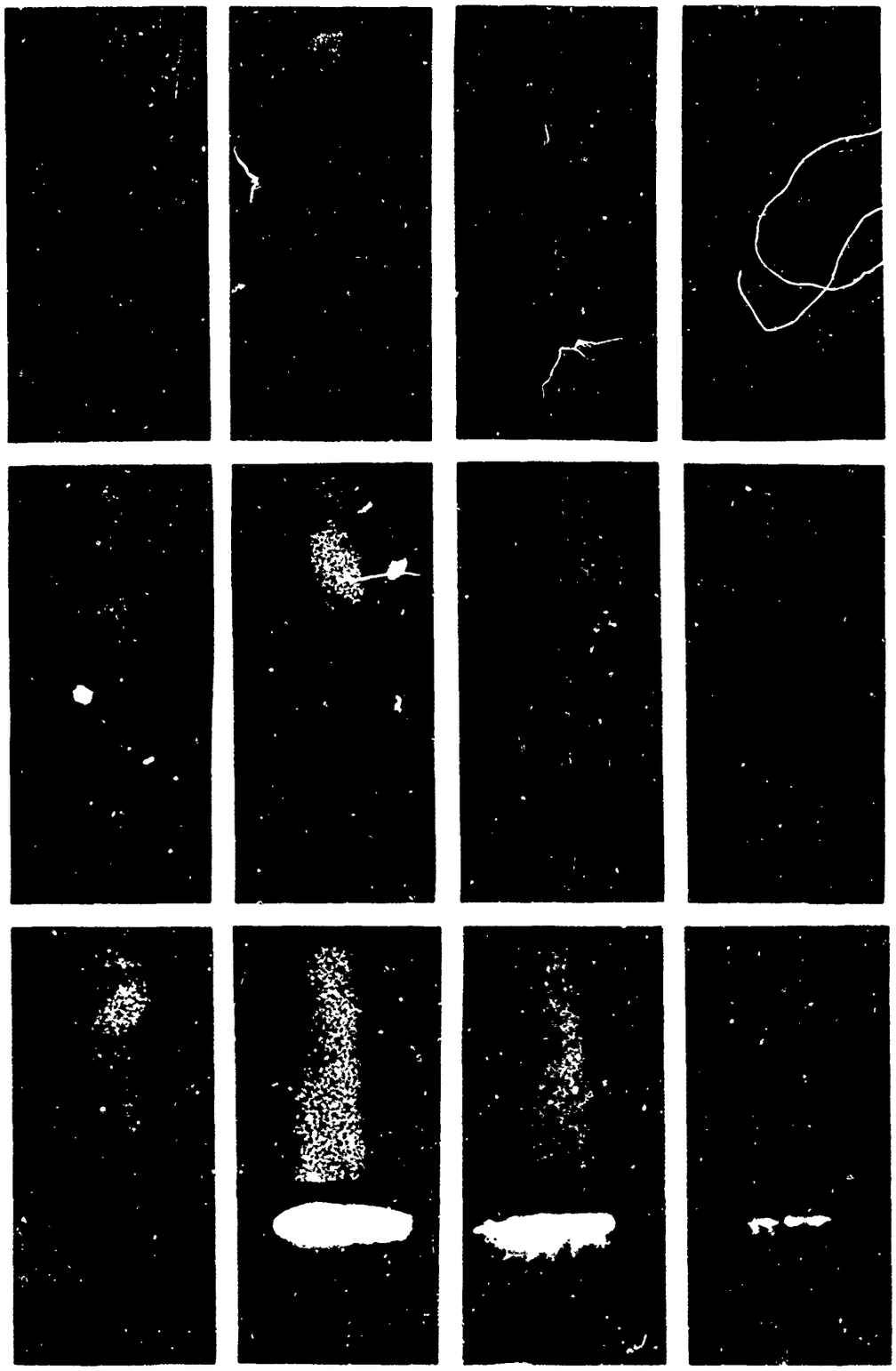

FIGURE B-14. Photographic Sequence for Test 14. (Mild steel, HEP-1, infinite air gap, unc[illegible]d.)

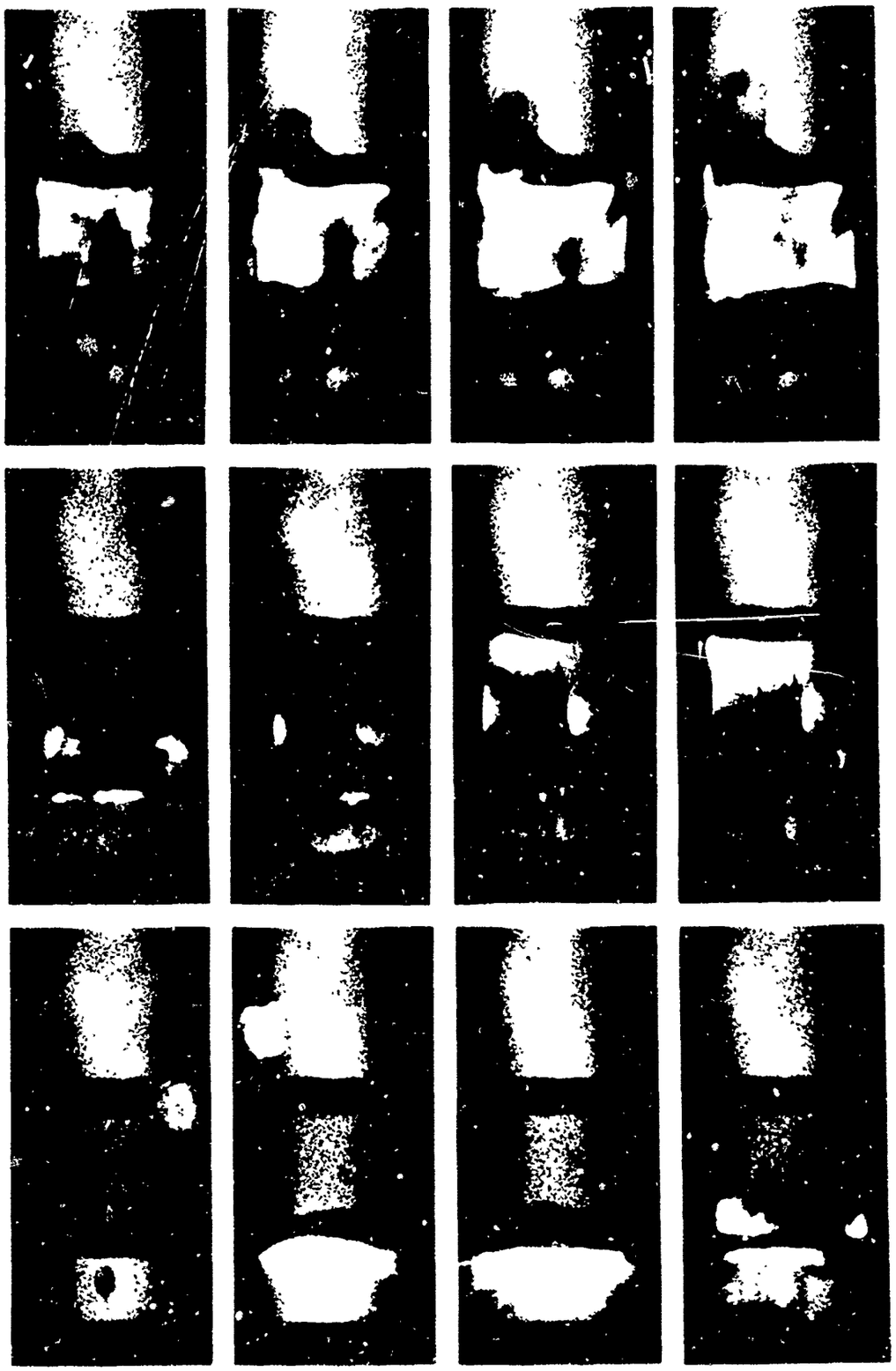

FIGURE B-15. Photographic Sequence for Test 15. (Mild steel, HEP-1, 3.0-inch air gap, HEP-1, mild steel.)

FIGURE B-16. Photographic Sequence for Test 16. (Hard steel, HEP-2, 3.0-inch air gap, HEP-2, hard steel.)

FIGURE B-17. Photographic Sequence for Test 17. (Hard steel, HEP-2, 2.5-inch air gap, HEP-2, hard steel.)

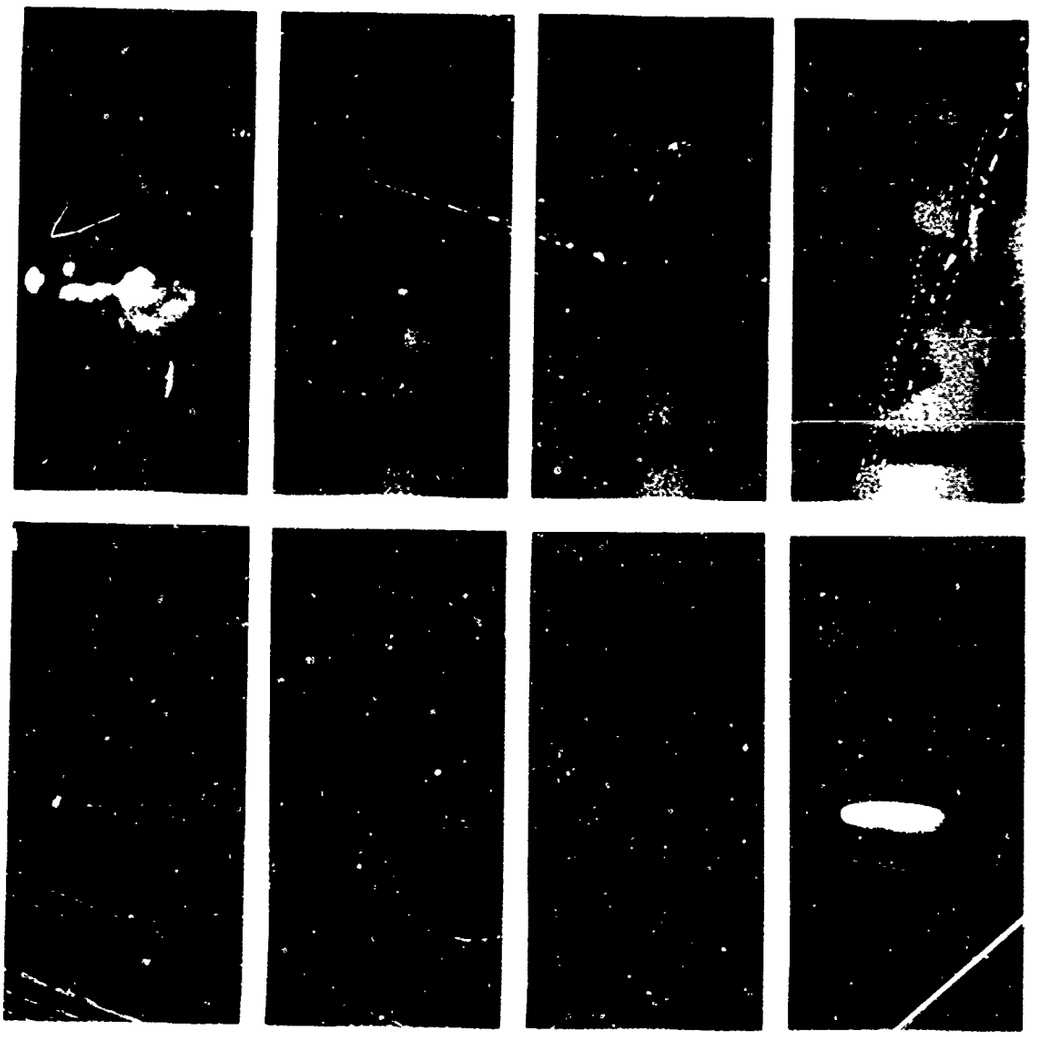

FIGURE B-18. Photographic Sequence for Test 18. (Hard steel, HEP-2, 2.0-inch air gap. HEP-2, hard steel.)

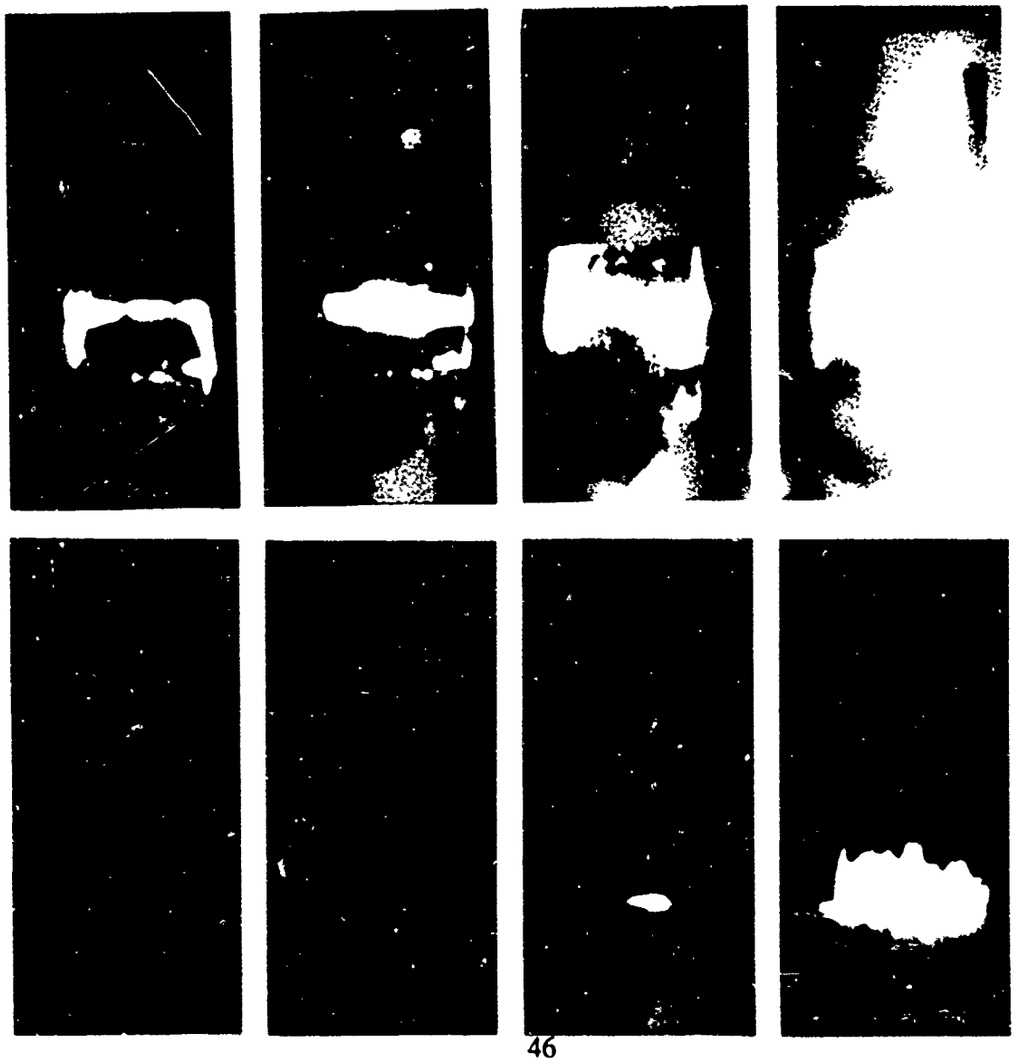

FIGURE B-19. Photographic Sequence for Test 19. (Hard steel, HEP-2, 0.75-inch air gap, HEP-2, hard steel.)

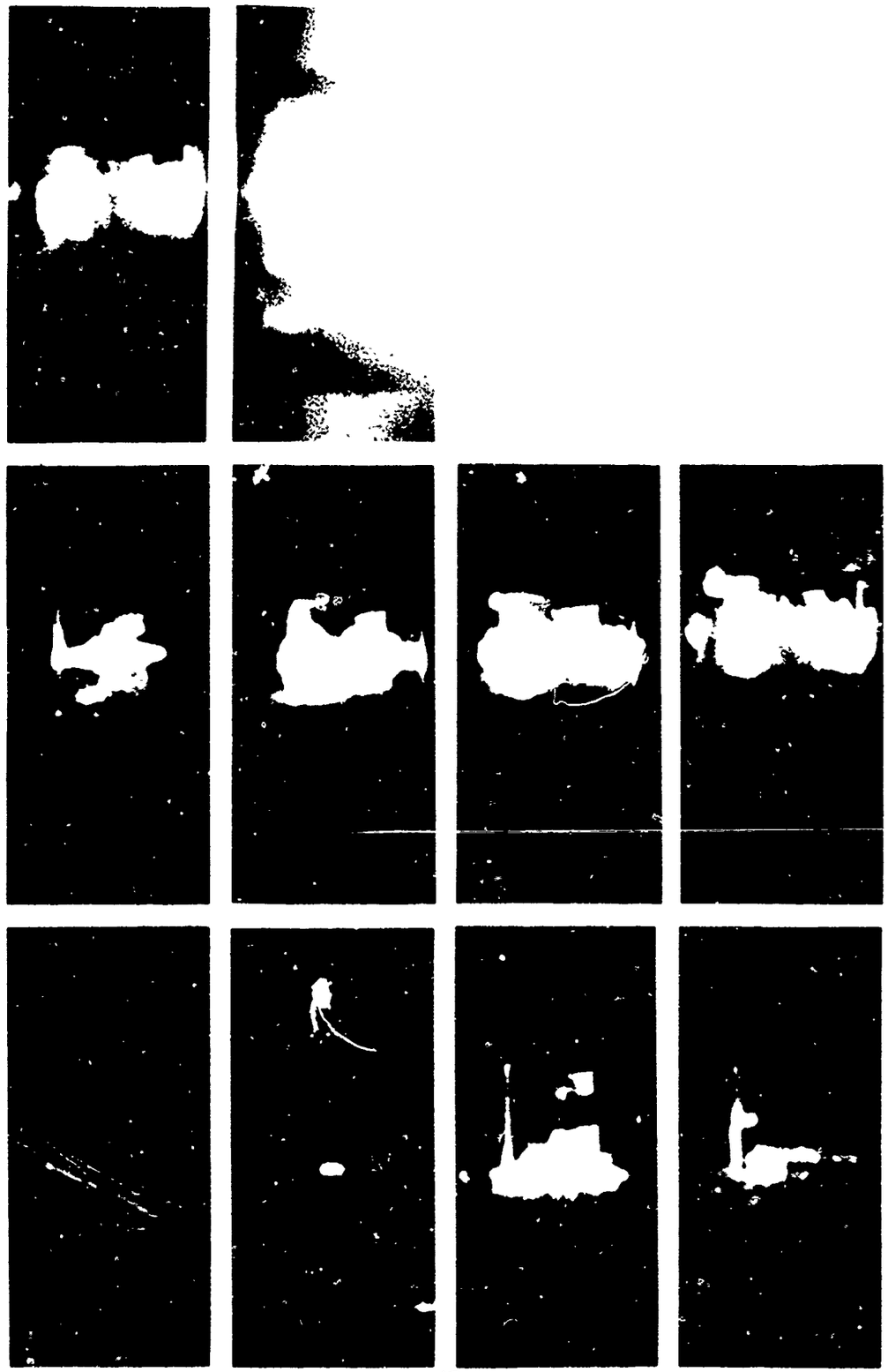

FIGURE B-20. Photographic Sequence for Test 20. (Hard steel, HEP-2, 0.5-inch air gap, HEP-2, hard steel.)

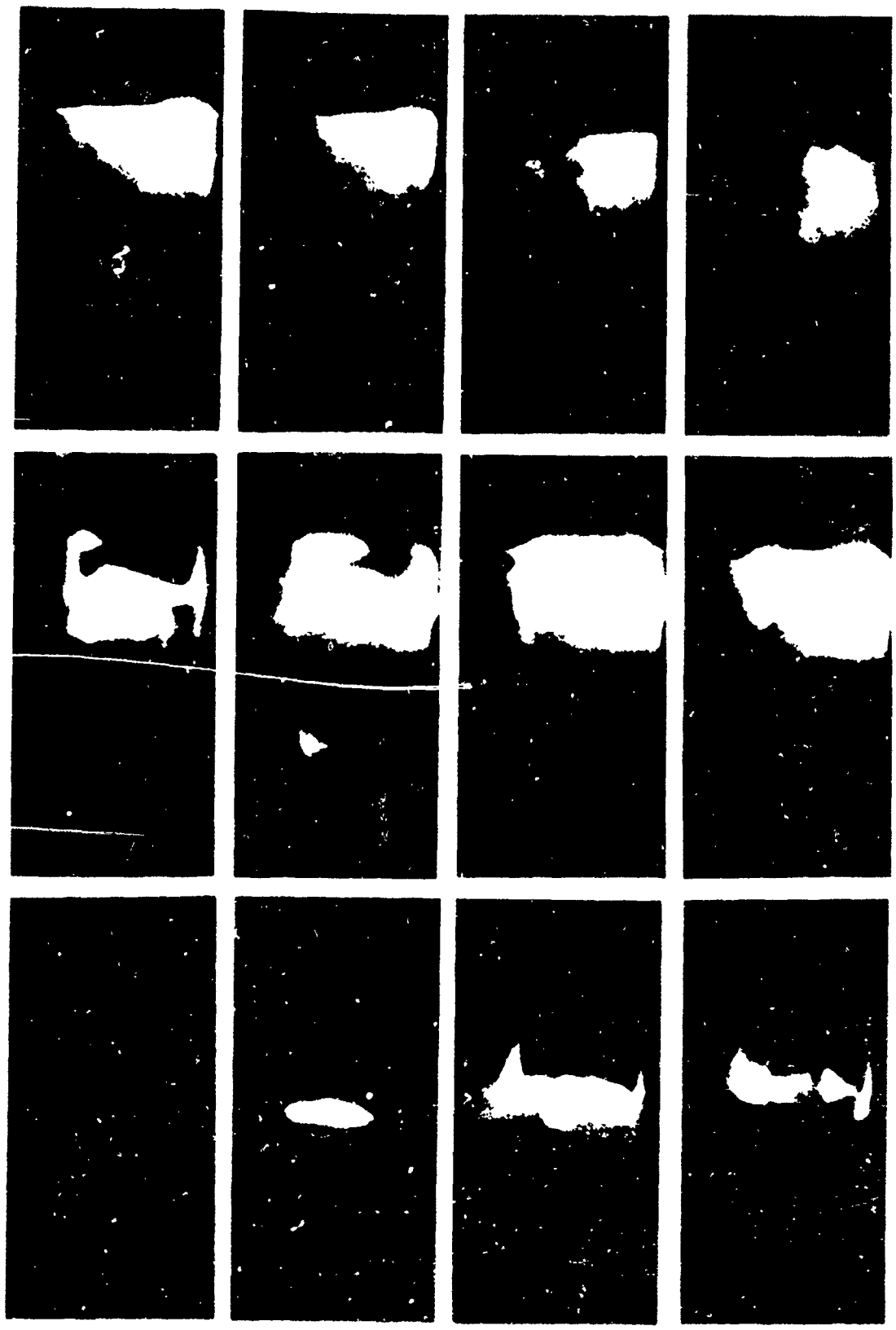

FIGURE B-21. Photographic Sequence for Test 21. (Hard steel, HEP-2, 0.25-inch air gap, HEP-2, hard steel.)

FIGURE B-22. Photographic Sequence for Test 22. (Hard steel, HEP-2, 1.5-inch air gap, inert, hard steel.)

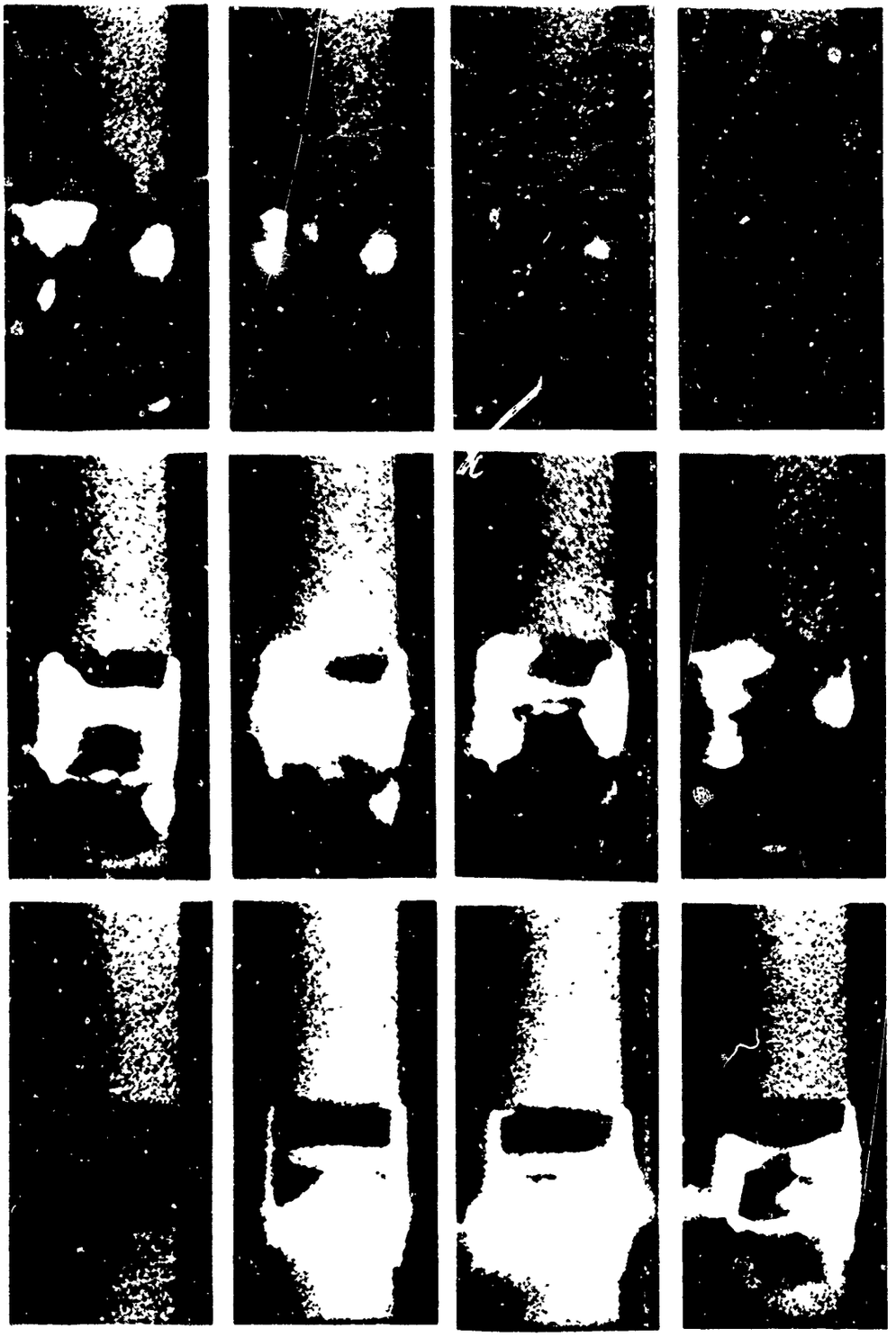

FIGURE B-23. Photographic Sequence for Test 23. (Hard steel, HEP-2, 1.0-inch air gap, inert, hard steel.)

INITIAL DISTRIBUTION

29 Naval Air Systems Command

AIR-05 (1)	AIR-5402B (1)	AIR-932F (1)
AIR-09F1 (1)	AIR-5402C (1)	AIR-932K (1)
AIR-4231 (1)	AIR-5402D (1)	AIR-933 (1)
AIR-5004 (2)	AIR-5403 (1)	APC-201 (1)
AIR-516C (1)	AIR-5404 (1)	PMA-242 (1)
AIR-540 (1)	AIR-54041 (1)	PMA-24251 (1)
AIR-5401B1 (1)	AIR-93 (1)	PMA-258 (1)
AIR-5401E (1)	AIR-931T (1)	PMA-259 (1)
AIR-5401F1 (1)	AIR-932 (1)	
AIR-5401H (1)	AIR-932D (1)	

13 Chief of Naval Operations

OP-03 (1)	OP-411F (1)	OP-954D (1)
OP-05 (1)	OP-506 (1)	OP-982E (1)
OP-098 (1)	OP-506G4 (1)	OP-982F7 (1)
OP-354 (1)	OP-55 (1)	
OP-411 (1)	OP-621C (1)	

6 Chief of Naval Research, Arlington
- OCNR-10P (1)
- OCNR-1131 (1)
- OCNR-1132 (1)
- OCNR-1132P, R. Miller (1)
- OCNR-1133 (1)
- OCNR-213 (1)

14 Naval Sea Systems Command

SEA-62 (1)	SEA-62Y13 (1)	SEA-6621 (1)
SEA-62D (1)	SEA-62Z (1)	SEA-6622, D. Porada (1)
SEA-62E (1)	SEA-66 (1)	SEA-666 (2)
SEA-62W (1)	SEA-662, R. Bowen (1)	Technical Library (2)

1 Commander in Chief, U. S. Pacific Fleet, Pearl Harbor (Code 325)
1 Commander, Third Fleet, San Francisco
1 Commander, Seventh Fleet, San Francisco
2 Naval Academy, Annapolis (Director of Research)
2 Naval Ordnance Station, Indian Head
- Code 2031, P. Dendor (1)
- Code 5246, Technical Library (1)

2 Naval Research Laboratory
- A. Williams (1)
- Technical Information Section (1)

4 Naval Surface Warfare Center, Dahlgren
- Code G-13, D. Dickinson (1)
- Code G-22, T. Swierk (1)
- Code G-302, W. Soper (1)
- Technical Library (1)

2 Naval Surface Warfare Center, Indian Head Detachment, Indian Head
- Code R-10E, J. Kelly (1)
- Code R-16, A. Toma (1)

10 Naval Surface Warfare Center, White Oak Laboratory, Silver Spring
- Code R-10C, L. Roslund (1)
- Code R-10H, M. Swisdak (1)
- Code R-11
  - C. Gotzmer (1)
  - N. Johnson (1)
- Code R-12, L. Montesi (1)
- Code R-13
  - R. Bernecker (1)
  - S. Coffey (1)
  - C. Dickinson (1)
- Code R-16, J. Corney (1)
- Technical Library (1)

1 Naval War College, Newport

1 Naval Weapons Station, Yorktown (Code 50)
1 Naval Weapons Support Center, Crane (Technical Library)
1 Office of Naval Technology, Arlington (ONT-20)
1 Army Missile Command, Redstone Arsenal (AMSMI-RD-PR-E, D. Dreitzler)
1 Army Armament Research, Development and Engineering Center, Picatinny Arsenal (Technical Library)
3 Army Ballistic Research Laboratory, Aberdeen Proving Ground
AMXBR-TED
R. Frey (1)
P. Howe (1)
SLCBR-TB-A, N. Rupert (1)
1 Army Research Office, Research Triangle Park (DEXTR-PP-LIB, D. Mann)
1 Air Force Academy, Colorado Springs (FJSRL/MC)
1 Air Force Astronautical Laboratory, Edwards Air Force Base (AFAL/MKPL, C. Merrill)
1 Air Force Inspection and Safety Center, Norton Air Force Base (Weapon Safety Office)
1 Air Force Intelligence Agency, Bolling Air Force Base (AFIA/INTAW, Maj. R. Esaw)
4 Air Force Munitions Systems Division, Eglin Air Force Base
AFATL/DLDE, G. Parsons (1)
AFATL/DLJW, J. Foster (1)
AFATL/DLODL, Technical Library (1)
MSD/YOI, J. Jenus (1)
1 Defense Advanced Research Projects Agency, Arlington (DARPA/MSD)
2 Defense Technical Information Center, Alexandria
1 Department of Defense, Explosives Safety Board, Alexandria (J. M.Ward)
6 Lawrence Livermore National Laboratory. Livermore, CA
MS L-282, E. Lee (1)
MS L-324, M. Constantino (1)
MS L-368
L. Green (1)
E. James (1)
C. Tarver (1)
A. Weston (1)
4 Los Alamos National Laboratory, Los Alamos, NM
MS-216, J. Dienes (1)
MS-J960, M-8
A. W. Campbell (1)
J. McAffee (1)
J. Ramsay (1)
4 Sandia National Laboratories, Albuquerque, NM
Div. 1510, J. Nunziato (1)
Div. 1512, M. Baer (1)
Div. 1533, M. Kipp (1)
Div. 2514, L. Weirick (1)
1 Applied Ordnance Technology, Columbia, MD (Pilot NIMIC)
1 Atlantic Research Corporation, Gainesville, VA (K. J. Graham)
2 Comarco, Incorporated, Ridgecrest, CA
R. G. S. Sewell (1)
A. Victor (1)
1 Hercules, Incorporated, Bacchus Works, Magna, UT (A. G. Butcher)
1 Hudson Institute, Incorporated, Center for Naval Analyses, Alexandria, VA (Technical Library)
1 Morton Thiokol, Incorporated, Huntsville, AL (W. B. Thomas)
1 The Johns Hopkins University, Applied Physics Laboratory, Laurel, MD (Chemical Propulsion Information Agency)

OF CENTER DISTRIBUTION

1 Code 01
1 Code 31
1 Code 32
1 Code 3205, F. Markarian
1 Code 3205I, S. Dessy
2 Code 3208
  C. Dattling (1)
  J. Fontenot (1)
1 Code 321, L. Josephson
1 Code 321, J. Baldwin
1 Code 3[illegible], M. McCubbin
1 Code 3201, E. Lundstrom
1 Code 327, R. Miller
4 Code 343 (3 plus Archives Copy)
2 Code 3686, GIDEP
1 Code 36871, J. Mathre
1 Code 37, J. Wunderlich
1 Code 372, T. Loftus
1 Code 38
1 Code 389
1 Code 38903
6 Code 3891
  A. Atwood (1)
  L. Boyar (1)
  M. Chan (1)
  C. Price (1)
  N. Pitcher (1)
  R. Reed (1)
104 Code 3894
  S. Finnegan (100)
  O. E. R. Heimdahl (1)
  A. Lindfors (1)
  M. Wagenhals (1)
  K. Woods (1)
1 Code 39